DEVELOPMENT OF A DETECTOR FOR TRACE AMOUNT OF NITROGEN DIOXIDE USING LIGHT EMITTING DIODE

BY

MOCH SYARIF ROMADHON

A Thesis Presented to the

DEANSHIP OF GRADUATE STUDIES

KING FAHD UNIVERSITY OF PETROLEUM & MINERALS

DHAHRAN, SAUDI ARABIA

In Partial Fulfillment of the
Requirements for the Degree of

MASTER OF SCIENCE

In

PHYSICS

May, 2015

KING FAHD UNIVERSITY OF PETROLEUM & MINERALS

DHAHRAN- 31261, SAUDI ARABIA

DEANSHIP OF GRADUATE STUDIES

This thesis, written by **Moch Syarif Romadhon** under the direction of his thesis advisor and approved by his thesis committee, has been presented to and accepted by the Dean of Graduate Studies, in partial fulfillment of the requirements for the degree of **MASTER OF SCIENCE IN PHYSICS.**

Dr.Abdul-Aziz Al-Jalal
(Advisor)

Dr. Abdullah A. Al-Sunaidi
Department Chairman

Dr.Khaled Gasmi
(Member)

Dr. Salam A. Zummo
Dean of Graduate Studies

Dr. Mohammed M. Faiz
(Member)

11/6/15

Date

This thesis is dedicated to my beloved family

ACKNOWLEDGMENTS

This thesis was funded by the National Plan for Science, Technology and Innovation (MAARIFAH) – King Abdulaziz City for Science and Technology – Through the Science & Technology Unit at King Fahd University of Petroleum & Minerals (KFUPM) – the Kingdom of Saudi Arabia, award number 12-ENV2365-04.

I offer my sincerest gratitude to my supervisor, Dr. Abdul-Aziz Al-Jalal, who has supported me throughout my thesis with patience and knowledge. I attribute the level of my Master degree to his encouragement and effort.

I am also grateful to the thesis committee member Dr. Khaled Gasmi and Dr. Muhammed Faiz and also optic lab member Dr. Watheq Ahmed Al-Basheer for an enthusiastic discussion and some correction in thesis draft.

In the various laboratories and workshops I have been aided in running the equipment by Sreedharan Pillai and Jun. a fine technician and machinist who has many surprised ideas when get stuck in the middle of research.

In my daily life during my study I have blessed with a friendly and cheerfully group of indonesian student. These people help me to bring the indonesian flavor in the Saudi Arabia.

Finally I would like to mention my beloved family in Indonesia who support me for taking graduate study. Especially for my wife, Mirda Ashfiani Husna, who has been patiently became a good listener during my master study even though her accounting background make me sure enough that she has no idea what I am talking about.

TABLE OF CONTENTS

LIST OF TABLES

LIST OF FIGURES

LIST OF ABBREVIATIONS

CCD Camera	:	Charge-Coupled Device Camera
DOAS	:	Differential Optical Absorption Spectroscopy
G	:	Gaussian function
LED	:	Light Emitting Diode
NO_2	:	Nitrogen dioxide
N_2	:	Nitrogen gas
nm	:	nanometer
O_2	:	Oxygen gas
P	:	pressure
ppm	:	part per million
ppb	:	part per billion
RRS	:	Rotational Raman scattering
T	:	Temperature
VRS	:	Vibrational Raman scattering
$\vec{a}$	:	parameter vector
a_s	:	Scaling factor
$A(\lambda)$	:	Instrumental effect and turbulence effect
C_n	:	Refractive index structure constant
c_j	:	Column density of gas j
h	:	Planck constant

$H(\lambda)$	:	Instrumental function
$I_o(\lambda)$	:	Incident light
$I(\lambda)$	:	Transmitted light
$I^*(\lambda)$	:	Convolved light
$I^{**}(\lambda)$	:	Discretized light
k	:	Boltzmann constant
n	:	Number of pixel
N	:	Number of molecule
$OD(i)$	:	Optical Density
$P(\lambda)$	:	Polynomial function
r_c	:	Deflected light beam radius
r_i	:	Incident light beam radius
$S(\lambda)$	:	Reference spectra
$S\_mea(\lambda)$	:	Measured reference spectrum
$S_{cal}(\lambda)$	:	Calculated reference spectrum
w	:	Monochromator resolution
$\delta(\lambda)$	:	Standard deviation
ε	:	Absorption coefficient
ε_R	:	Rayleigh coefficient
ε_M	:	Mie coefficient
σ	:	Gas absorption cross-section
σ_R	:	Rayleigh cross-section
σ_M	:	Mie cross-section

ABSTRACT

Full Name : Moch Syarif Romadhon

Thesis Title : Development of a Detector for Trace amount of Nitrogen Dioxid using Light Emitting Diode

Major Field : Physics

Date of Degree : May 2015

A setup based on Differential Optical Absorption Spectroscopy method is developed to detect trace amount of NO_2 gas. A labview program is coded to control and collect the data and a Mathematica code is written to read and analyze the data. The components of the setup are a commercial white LED used as the light source, a 15-cm gas cell, a high resolution monochromator Horriba SPEX500M, coupled to a 3000-pixel CCD line camera Thorlab LC1-USB CCD. Two NO_2 gas concentrations, 206 ppm and 2.6 ppm, are used to check the performance of the setup and the measurements are found to agree very well with the quoted concentrations by the gas cylinder supplier. The deviation of the measurements from the quoted values for the case of the 206 ppm is less than 0.4 % while for the case of the 2.6 ppm is less than 8%. The detection limit is estimated to be ~ 1.2 ppm. This limit is equivalent to ~ 0.6 ppb for a path length of 300 m which is much less than the 50 ppb long-term exposure safe limit to NO_2 gas.

ملخص الرسالة

الاسم الكامل : سيرف رمضان

عنوان الرسالة : تطوير مستقبل للتراكيز الصغيرة من غاز ثاني اكسيد النيتروجين لاستخدام الدايود الضوئي

التخصص : فيزياء

تاريخ الدرجة العلمية: مايو : ٢٠١٥

لقد تم تطوير جهاز يعمل على مبدأ مطيافية الفرق في الامتصاص الضوئي لاستكشاف التراكيز الصغيرة من غاز ثاني اكسيد النيتروجين حيث تم كتابة برنامج اللاب فيو للتحكم وجمع القياسات كذلك تم استخدام برنامج الماثماتيكا لقراءة وتحليل القياسات. مكونات هذا الجهاز هي دايود ابيض تجاري كمصدر للضوء بالاضافة لخلية غاز بطول 15 سم ومحلل أطياف أحادي الطول الموجي متصل مع كاميرا ذات 3000 بكسل من شركة ثورلابس. تم استخدام تركيزين من الغاز هما 206 جزء بالمليون وكذلك 2.6 جزء بالمليون للتحقق من دقة القراءات حيث أن كلا التركيزين متطابقين مع تراكيز الشركة الصانعة للغاز. عند استخدام تركيز 206 جزء بالمليون وجد انحراف في القياس بحدود 0.4 % مقارنة مع تركيز الشركة الصانعة للغاز في حين أن الانحراف في حالة تركيز 2.6 جزء بالمليون كان أقل من 8 %. لقد وجد أن أقل تركيز يمكن قياسه هو 1.2 جزء بالمليون وهذا التركيز يقابل 0.6 جزء بالبليون في مسار طولي بطول 300 متر وهو تركيز أقل بكثير من 50 جزء بالبليون وهو الحد المسموح به للتعرض بدون اضرار.

CHAPTER 1

INTRODUCTION

In the atmosphere, nitrogen dioxide (NO_2) is one of the six principal air pollutants [1]. NO_2 gas is produced in high temperature condition in the combustion processes of fossil fuel in cars, trucks and buses, and off-road equipment [2]. In addition, small amount of this gas is produced naturally by processes involving microbial in the soil or water bodies and lightning [3]. Its concentration in the ambient air ranges from 0 to 150 ppb [4]. Unfortunately, several health problems are linked to long term exposure of small concentration higher than 50 ppb of NO_2 [5]. Based on this fact, the availability of sensitive NO_2 gas sensor is important for preventing damages caused by NO_2 gas.

1.1 Challenge in Atmospheric Trace Gas Measurement

Useful measurement technique of atmospheric trace species should fulfill several requirements. First, they must be sufficiently sensitive to detect the species under consideration at their ambient concentration levels. This can be a very demanding criterion; for instance, species present at mixing ratios ranging from as low as 0.1 ppt to several ppb can have significant influence on atmospheric chemistry [6].

Second, it is equally important for measurement technique to be specific, which means that the result of the measurement of a particular species must be neither positively nor

negatively influenced by any other trace species simultaneously present in the probed volume of air.

Third, Design of detector should be simple, capable of real time operation and portable. Since atmospheric measurement often deal with complicated environment topography, these practical requirement need to be considered.

1.2 The Need for this Research

To date, no single measurement technique can fulfill all the requirements; therefore, in a particular application the selection of a technique will be based on the specific requirements: What species are to be measured? Is it necessary to determine several gas species simultaneously? What is the required accuracy, time resolution, and spatial resolution? Other aspects to be considered are logistic requirement like power consumption, mounting of light sources or retro-reflectors.

Of several techniques for measuring in situ NO_2 gas, chemiluminescence is the most prevalent method [7]. It is based on the chemiluminescence reaction of NO with O_3 to form electronically excited NO_2, which fluoresces at visible and near infrared wavelengths. This technique is simple and relatively reliable. It also provides high sensitivity down to 1 ppb. But, it is localized to specific location and requires a routine maintenance for optimum performance.

Differential Optical Absorption Spectroscopy (DOAS) is a well-established measurement technique for the analysis of NO_2 gas with the possibility of detecting additional gases simultaneously with relatively high accuracy in a real time. This technique is based on

measuring light absorption by NO_2 gas in spectral range 350 – 450 nm over a long path. The path length can be hundreds meters up to several kilometers. Hence, this method measures gas concentration over long range and it requires less maintenance for operation than device based on chemiluminescence.

The aim of this research is to develop of an NO_2 gas detector based on DOAS method using Light Emitting Diode (LED) as light source. LEDs have properties which make them a suitable DOAS light source: They have continuous broad band emission, long lifetimes and low power consumption. This work employs an LED with emission spectra at blue wavelength (400-470 nm) to detect NO_2 gas.

1.3 Objective

The objective of this research is to develop an NO_2 gas detector based on DOAS using an LED as a light source with detection limit better than 3 ppm of NO_2/N_2 gas mixture in a 15.5 cm gas cell. This detection limit is equivalent to 1.6 ppb over 300 m path length.

CHAPTER 2

Background

In this chapter, the following will be discussed: some relevant physical and chemical properties of NO_2 gas, a recent review of DOAS method and a mathematical description of DOAS method.

2.1 Nitrogen Dioxide in the Troposphere

Nitrogen dioxide NO_2 and nitrogen monoxide NO have an important role in the chemical processes in the troposphere. The troposphere is the lowest layer of atmosphere extends from the earth surface up to 10 km. NO_2 and NO undergo a series of reactions that eventually lead to formation of nitric acid HNO_3 which is the main component of acid rain besides sulfuric acid H_2SO_4. They also take part in ozone O_3 formation as a catalyst.

Nitrogen oxides are created by a reaction of atomic oxygen O with molecular nitrogen N_2

$$O + N_2 \rightarrow NO + N \quad (1).$$

In the atmosphere, this reaction can take place whenever air is heated higher than 2000 K. This thermal energy is sufficient to dissociate molecular oxygen O_2 into atomic oxygen O. NO molecule which is produced from reaction 1 is oxidized quickly by ozone into NO_2:

$$O_3 + NO \rightarrow NO_2 + O_2 \quad (2).$$

NO_2 can also be photolyzed by UV radiation producing NO molecule and excited atomic oxygen $O(^3P)$.

$$NO_2 \xrightarrow{hv\ (\lambda<420\ nm)} NO + O(^3P) \quad (3).$$

$O(^3P)$ reacts quickly with O_2 yielding ozone molecule:

$$O(^3P) + O_2 + M \rightarrow O_3 + M \quad (4),$$

with M is a collision molecule (e.g. N_2 or O_2).

NO_2 molecule is decomposed by hydroxyl radical (OH) into nitric acid HNO_3

$$NO_2 + OH + M \rightarrow HNO_3 + M \quad (5).$$

This reaction will reduce both NO_2 and OH composition in the atmosphere and at the same time it produces HNO_3 which is one of the main components of acid rain. Hydroxyl radical concentration is influenced by sun's radiation hence the life time of NO_2 varies according to daylight duration. In the summer time, NO_2 last for 12 hours while in the winter it last for 33 hours [8].

Another possible reaction is the oxidation of NO_2 into NO_3

$$NO_2 + O_3 \rightarrow NO_3 + O_2 \quad (6).$$

This NO_3 molecule can be reduced by photolysis in two ways:

$$NO_3 \xrightarrow{hv} NO + O_2 \quad (7),$$

$$NO_3 \xrightarrow{hv} NO_2 + O \quad (8).$$

Beside this photolysis reaction, reduction of NO_3 is taken place by a reaction with NO:

$$NO_3 + NO \rightarrow 2NO_2 \quad (9).$$

During daylight, these photolysis processes reduce the concentration level of NO_3 significantly. While in the night, accumulation of NO_3 occurs due to lack of photolysis processes and low concentration of NO.

Additionally, NO_3 can react with NO_2 yielding N_2O_5:

$$NO_3 + NO_2 + M \leftrightarrow N_2O_5 + M \quad (10).$$

N_2O_5 reacts with water surfaces to form HNO_3. Thermodynamic equilibrium among these three molecules (NO_3, NO_2 and N_2O_5) depends strongly on atmosphere temperature.

2.2 NO_2 Absorption Cross-section

NO_2 molecules can present in many different states according to their energy, parity, angular momentum and electronic configuration [9]. Transition from one state to another is frequently associated with absorption or emission of electromagnetic radiation.

The excitation of a molecule NO_2 in the ground state to an exited state NO_2* induced by the absorption of a photon with energy hv is called photoabsorption of NO_2

$$hv(E) + NO_2 \rightarrow NO_2^* \quad (11).$$

The probability of this transition can be expressed in terms of absorption cross section σ which is a function of radiation wavelength. Potential curves of low lying electronic states of NO_2 molecules is shown in Fig.1 [10] and the absorption in the blue region of the visible spectrum is due mainly to the $^2B_1 \leftarrow {}^2A_1$ transition. The absorption cross section for this transition in the wavelength range 250 nm to 800 nm is shown in Fig.2 [11]. The inset figure is an expanded view for the range between 435 nm to 465 nm which will be used in this work.

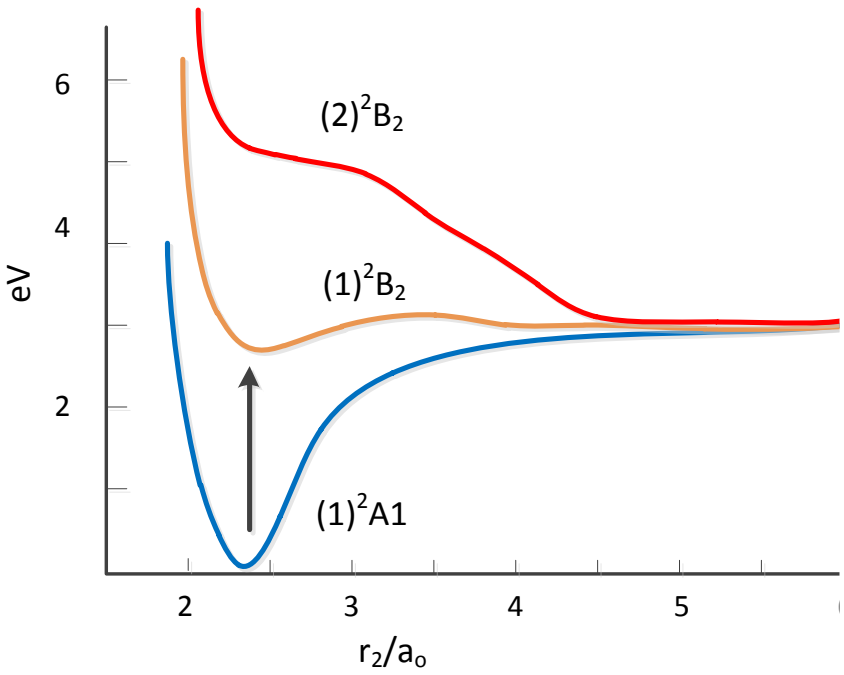

Figure 1 Potential energy curves of NO_2 electronic states drawn along the ON-O dissociation coordinate where r_2 is the distant between NO and O and a_o is Bohr radius [10].

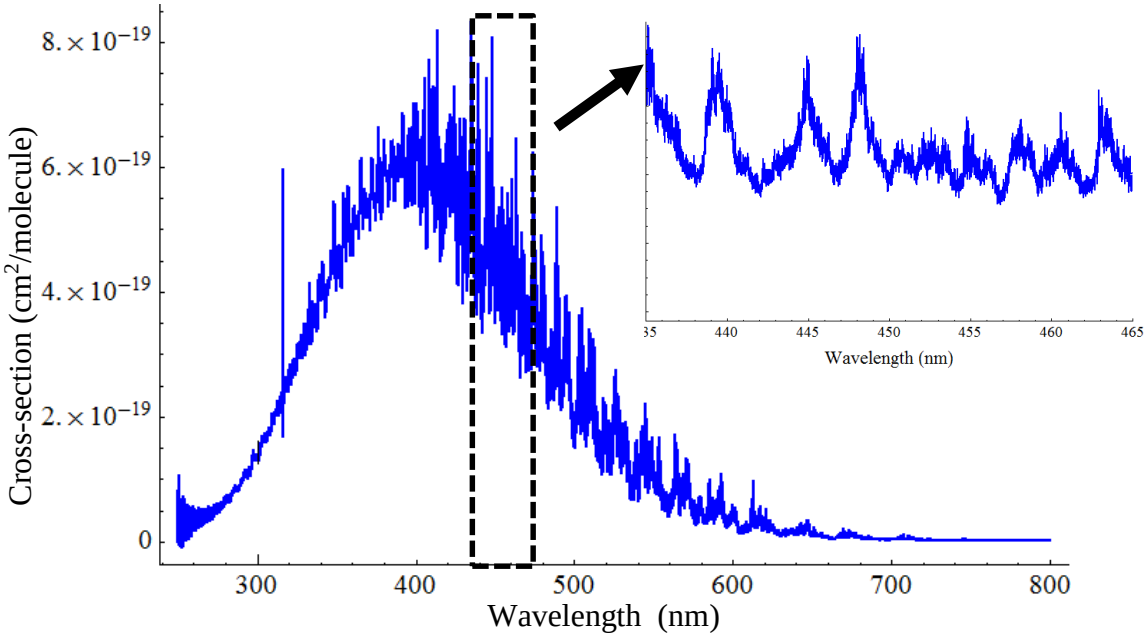

Figure 2 High resolution of NO_2 absorption cross section ranges from 250 nm to 800 nm [11]. The inset figure is an expanded view for the range from 435 nm to 465 nm which will be used in this work.

2.3 Radiation Transport in the Atmosphere

Trace gases measurement based on absorption processes have considerable advantages, such as low power consumption and potential for remote sensing. The basic challenges of this technique are radiation extinction in open atmosphere and scattered light production due to collision with atmospheric particles. This section discusses physical processes that affect radiation intensity during traveling in the open atmosphere.

2.3.1 Absorption

In absorption energy is removed from radiation field and converted into some other forms of energy such as heat [13]. After traversing an absorbing layer of thickness dl, the intensity of incident light I is changed by dI given by:

$$dI = -I(\lambda)\sigma_a(\lambda)\, N\, dl \quad (12),$$

or

$$dI = -I(\lambda)\varepsilon_a(\lambda)\, dl \quad (13),$$

where σ_a is the absorption cross-section of the molecule and N is the number of molecule per unit volume,$\varepsilon_a \equiv \sigma_a N$ is the absorption coefficient.

If light with intensity I_o traverses a cell of length L as shown in Fig. 3, the transmitted intensity I can be found by integrating Eq. 13 over the light path length L which leads to the well-known Beer-Lambert's Law

$$I(\lambda) = I_o(\lambda)Exp[-\sigma_a(\lambda)\alpha] \quad (14),$$

with

$$\alpha = \int_0^L N\, dl \quad (15).$$

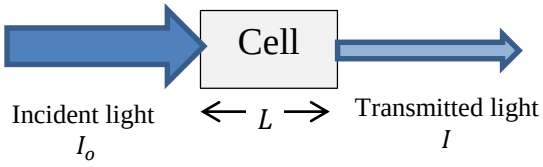

Figure 3 Absorption of light

2.3.2 Rayleigh scattering

Elastic scattering by particles much smaller than the wavelength of radiation is called Rayleigh scattering[14]. In general, the effect of scattering process to the transmitted light intensity depends on the size of light beam. Based on the size of the light beam, we can distinguish two extreme cases, as illustrated in Fig. 4: the wide beam case, for example, the illumination of the earth's atmosphere by the sun, and the narrow beam case, for example, the artificial light beam used in DOAS.

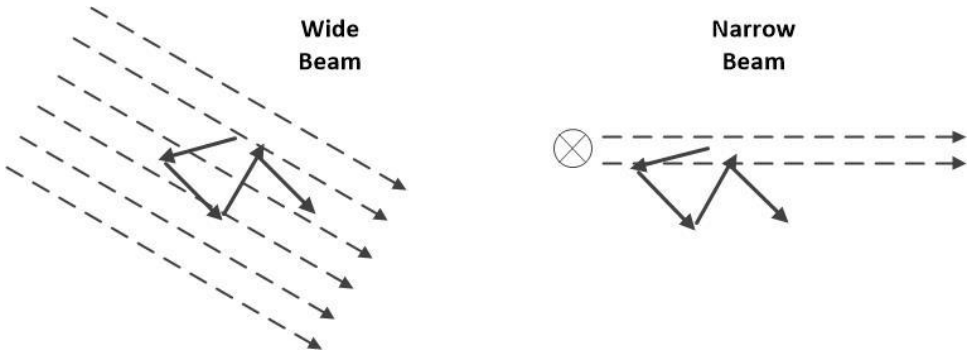

Figure 4 Difference between Wide Beam (Left) and Narrow Beam (right). In narrow beam, scattered photon has a little probability back to the beam, meanwhile in wide beam, the proportion of scattered photon is small compared to the beam

For the wide beam, number of photon in lateral direction (i.e. perpendicular to the beam) can be neglected, so scattering has a little effect to the overall incoming light intensity.

On the other hand, for the narrow beam, the possibility of photon to be scattered back into light beam is small. For this reason, we treat a Rayleigh scattering as an absorption process. The Rayleigh scattering cross-section $\sigma_R(\lambda)$ in cm^2 is given by [15]

$$\sigma_R(\lambda) = \frac{24\pi^3}{\lambda^4 N_{air}^2} \frac{(n_o(\lambda)^2 - 1)^2}{(n_o(\lambda)^2 + 2)^2} F_K(\lambda) \quad (16),$$

$$\sigma_R(\lambda) \approx \frac{8\pi^3}{3\lambda^4 N_{air}^2} (n_o(\lambda)^2 - 1)^2 F_K(\lambda) \quad (17),$$

where λ denotes the wavelength in cm, $n_0(\lambda)$ is the wavelength-dependent index of refraction of air, N_{air} is the number density of air (e.g 2.4×10^{19} molecules.cm^{-3} at 20° C, 1 atm), and $F_K \approx 1.061$ is a correction for anisotropy (polarizability of air molecules).

For simple estimates, the Rayleigh scattering cross-section can be written as:

$$\sigma_R(\lambda) = \sigma_{RO}\, \lambda^{-4} \quad (18),$$

$$\sigma_{RO} = 4.4 \times 10^{-16}\, cm^2 nm^4 \ \ (air) \quad (19).$$

The Rayleigh extinction coefficient $\varepsilon_R(\lambda)$ is given by:

$$\varepsilon_R(\lambda) = \sigma_R(\lambda)\, N_{air} \quad (20).$$

2.3.3 Mie scattering

Radiation scattering by particulates that have dimensions comparable or larger than the radiation wavelength is called Mie scattering. This scattering is less wavelength dependent than Rayleigh scattering and can be treated as absorption process for narrow beam with the extinction coefficient [15]:

$$\varepsilon_M(\lambda) = \varepsilon_{M0}\, \lambda^{-\alpha} \quad (21),$$

with the Angstrom exponent α is typically found in the range 0.5-2.5. Table 1 lists typical cross-sections for Rayleigh and Mie scatterings at different wavelengths.

Table 1. Typical Mie scattering coefficients and Rayleigh scattering coefficients. [15]

Wavelength (nm)	Rayleigh Scattering cross-section σ_R (10^{-26} cm^2)	Rayleigh Coefficient ε_R (10^{-5} m^{-1})	Typical Mie Scattering coefficient ε_M (10^{-5} m^{-1})
300	5.653	13.524	5.8
400	1.672	4.013	4
500	0.672	1.612	3
600	0.317	0.760	2.4

2.3.4 Raman Scattering

Raman scattering is an inelastic scattering in which the photon energy is transferred from the photon to a molecule (stokes line) or vice versa (Anti-stokes line). The term rotational Raman scattering (RRS) is used if only the rotational excitation is affected, if the vibrational state also changes, the term vibrational Raman scattering is used (VRS). Comparison of the total cross-section for the different Raman scattering types can be seen in Table 2 [16]. These cross-sections are very small and Raman scattering is neglected in this work.

Table 2. Cross-sections for different contributions to Raman scattered light. Absolute values are listed as well as relative contribution compared to RRS. N_2/O_2 is a gas mixture with mixing ratio 80% N_2 and 20% O_2. The cross-sections were calculated at 433 nm for RRS and 393 nm for VRS.[16]

Scattering type	**Cross-section (cm^2 sr^{-1} $molec^{-1}$)**	**Ratio (%)**
RRS (N_2/O_2)	3.4 x 10^{-29}	100
N_2 VRS	1. 2 x 10^{-30}	3.47
O_2 VRS	3.4 x 10^{-31}	1

2.3.5 Thermal Emission

Thermal emission from air molecules and aerosol particles at any given wavelength cannot exceed the Planck function for the temperature T of the atmosphere [15]. The thermal emission of a volume element with a length of ds is

$$I_{th}(\lambda, T) = \varepsilon_a(\lambda) I_p(\lambda, T) ds \quad (22),$$

where ε_a is the absorption coefficient, and $I_p(\lambda, T)$ is the Planck function.

$$dI_p(\lambda, T) = \frac{2hc^2}{\lambda^5} \frac{d\lambda}{\exp\left[\frac{hc}{\lambda kT} - 1\right]} \quad (23),$$

Here $h = 6.63 \times 10^{-34}\, Js$ is Planck constant, $c = 3 \times 10^8$ is speed of light, and $k = 1.38 \times 10^{-23}$ is Boltzmann constant.

At room temperature, noticeable thermal emission only takes place at infrared wavelengths and thermal emission is negligible in the blue region of visible spectrum. Thus, it is not considered in this work.

2.3.6 Atmospheric Turbulence

In the atmosphere, a light beam can be deflected by atmospheric turbulence as illustrated in Fig. 5. Turbulence is caused either by mechanical effects such as wind or thermal convection. The square of the average deflection of the beam center is given by the following empirical formula [15]

$$< r_c^2 >= 2.87 \frac{C_n^2 L^3}{r_i^{1/3}} \quad (24).$$

The refractive index structure constant C_n^2 ranges from 10^{-17} $m^{-2/3}$ (weak turbulence) to 10^{-13} $m^{-2/3}$ (strong turbulence). The radius of the beam is denoted by r_i and the length of the light path by L. For example, a light source radiation with a 10-m radius over a 10-km path has a deflection of 3.6 mm and 0.36 m for weak and strong turbulence, respectively. In this work, the turbulence effect is neglected due to the short length of the gas cell.

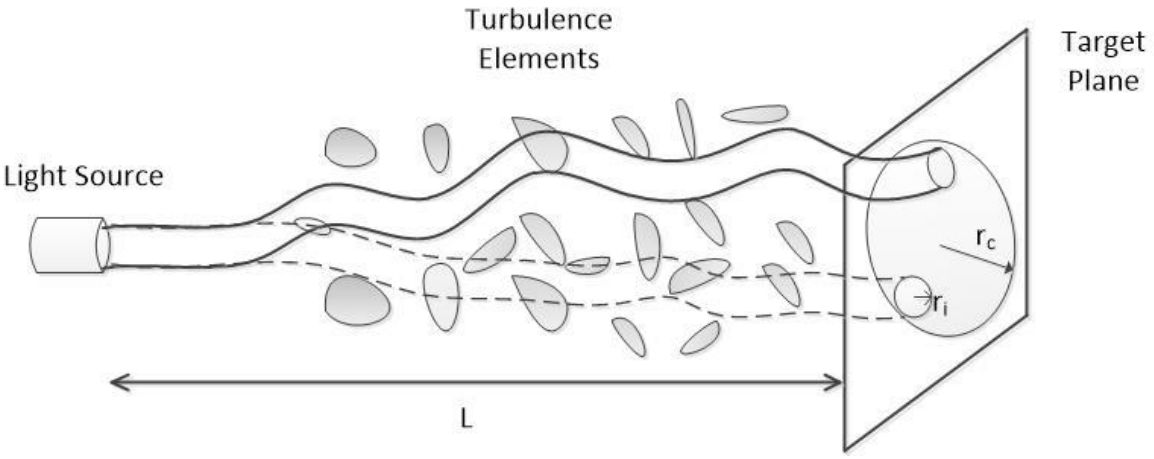

Figure 5 Light beam with radius r_i is deflected by atmospheric turbulence in the region within radius r_c

2.3.7 Radiation Transport Equation

Finally, a comprehensive description of atmospheric extinction in the presence of trace gases species can be expressed as:

$$I(\lambda) = I_o(\lambda) \exp\left[-L \sum_j \sigma_j(\lambda) c_j + \varepsilon_R(\lambda) + \varepsilon_M(\lambda)\right] \qquad (25).$$

Raman scattering, thermal emission and turbulence are neglected due to their small contributions compared to that of the gas absorption, Rayleigh and Mie scattering.

2.4 DOAS Overview

DOAS is a well-established method which has been used widely in detecting atmospheric gas traces. This method was introduced by Platt [17] in 1979 for measuring nitrous acid using an artificial light source. After this successful measurement, numerous detectors based on DOAS have been built for various trace gases, such as CH_2O [18], NO_3 [19], BrO [20], IO [21], NO_2 [22] and CHOCHO [23].

DOAS method is based on identifying the characteristic absorption of light after traversing a gas volume. Spectral position of absorbing peaks and their strength can be used to trace gas identification and quantification. DOAS method is able to remotely measure gas concentration in an open atmosphere which makes it a suitable method to detect highly reactive species such as NO_3, OH, NO_2 and halogen oxides.

The DOAS method can be applied in a wide variety of light path arrangements and observation modes. According to their light sources, we distinguish between active and passive DOAS [24]. Active DOAS uses artificial light, while passive DOAS relies on natural light sources, such as light from the sun, the moon or stars. Fig. 6 shows some experimental arrangements which illustrate the breadth of DOAS configurations that are in use today. Fig.6(a) shows a long-path (LP) arrangement in which an artificial light source is directly pointed to the detector. In Fig.6(b), several reflectors are used for vertical profiling. And Fig.6(c) shows a folded path DOAS arrangement using mirrors. The arrangements in the Fig.6(a)-6(c) demonstrate an active DOAS while a passive DOAS arrangement is shown in Fig.6(d) using the sun light as the light source.

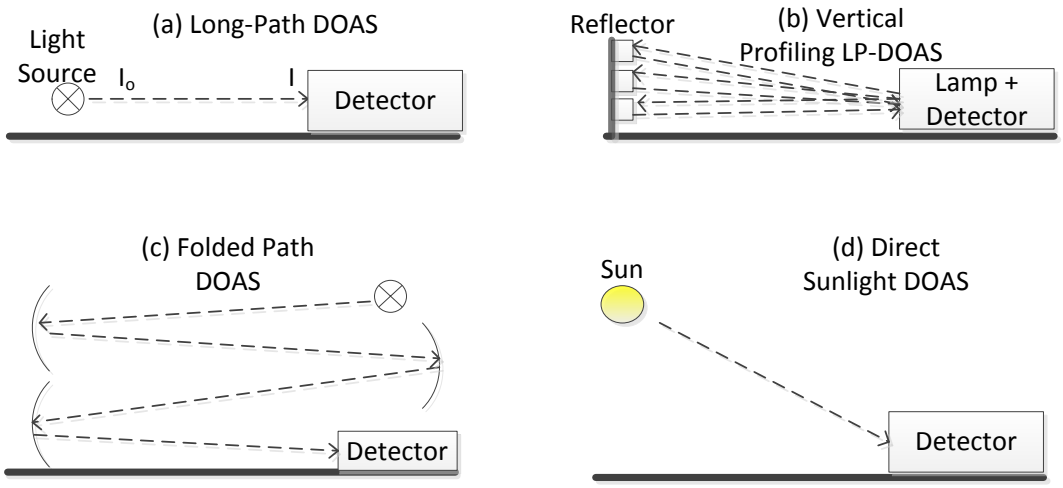

Figure 6 Various DOAS measurement system. (a),(b) and (c) are examples of active DOAS setup and (d) is a passive DOAS setup.

2.5 Selectivity, Precision and Accuracy of DOAS Approach

Performance of an analytical method can be determined by three aspects: selectivity, precision and accuracy.

Selectivity is the capability of the analytical method to distinguish among different trace gases in a measurement. Since DOAS relies on identifying the characteristic absorption spectrum of molecules, it provides an excellent selectivity. As shown in Fig.7, each gas has a unique characteristic absorption spectrum.

Precision of a DOAS measurement is influenced by atmospheric conditions as well as some properties the measuring instrument. The most common source that limits the precision is the shot noise which is a random error originating from random arrival of photons. This noise can be reduced by either increasing light intensity or integration time. If the main

source of noise in a signal is the shot noise, the signal-to-noise ratio is proportional to square root of the signal intensity.

Determination of DOAS accuracy is challenging since it requires knowledge of true concentration. This accuracy can be estimated by passing a light through known gas concentration. This technique could be applied because DOAS method does not induce a chemical transformation of measured gas.

In summary, DOAS is a highly versatile, selective, and accurate technique. In principle, a DOAS measurement is a “spectral photograph” of the atmospheric composition that allows the identification of its components and also determination of their concentration.

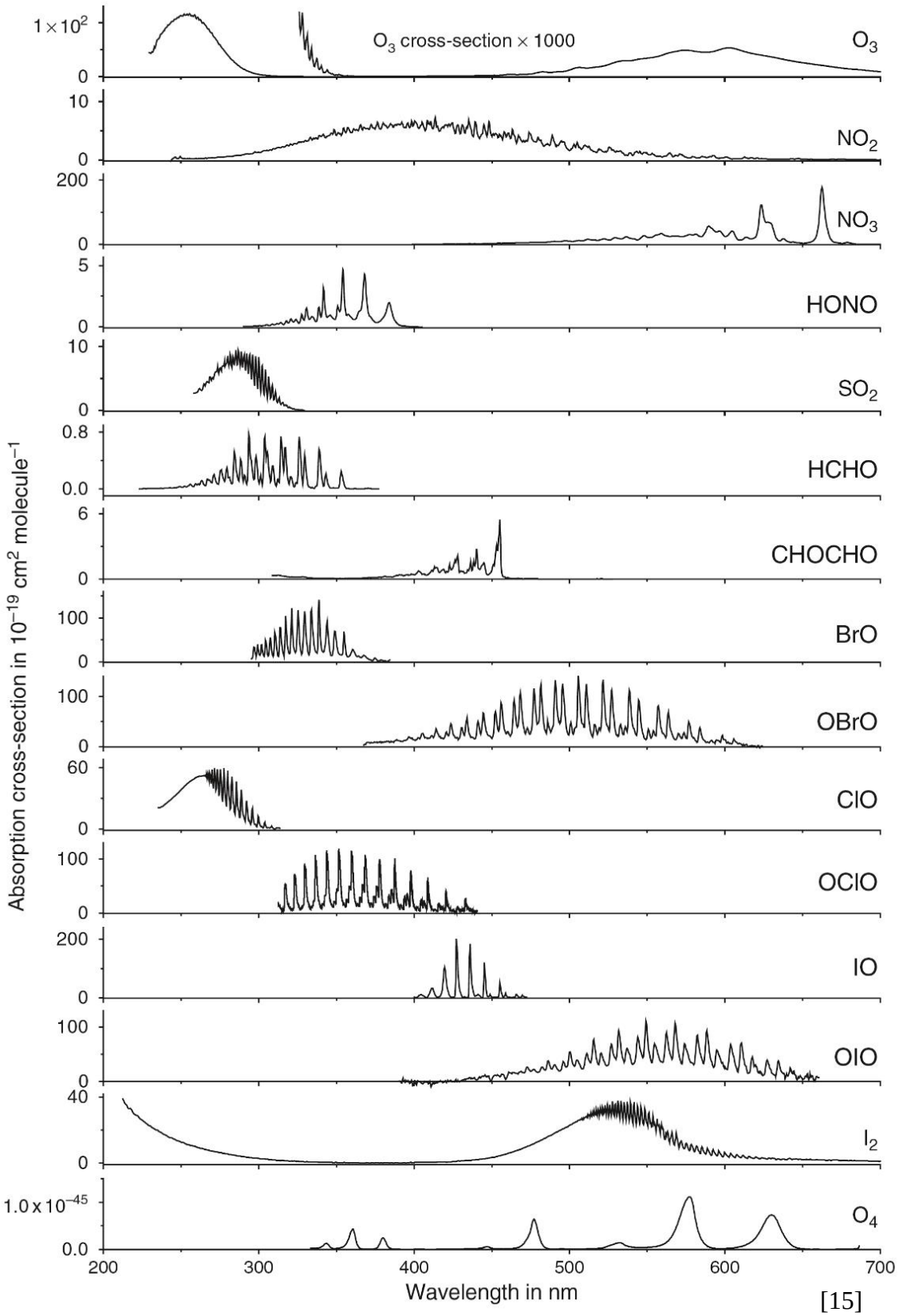

[15]

Figure 7 Absorption cross-section of some atmospheric gases species.

2.6 Mathematical Description of DOAS

In this section, we will discuss mathematical description of DOAS including its basic principle and method for gas concentration extraction.

2.6.1 DOAS Principle

From section 2.3, we know that in the open atmosphere, radiation transport is affected at least by three dominant processes. An effective analytic method should provide a way to separate these contributions. In DOAS, this separation is done by using the fact that the Rayleigh and Mie scatterings as well as turbulence cause a slow variation of the transmitted light with wavelength while the absorption by gas species causes a relatively rapid variation in intensity of the transmitted light. These variations create two distinct features in the signal spectrum: broad band feature and narrow band feature as shown in Fig.8. These slow and fast feature can be expressed as follow

$$I(\lambda) = \underbrace{I_o(\lambda)\exp[\varepsilon_R(\lambda)+\varepsilon_M(\lambda)]\,A(\lambda)}_{\text{Broad band feature}}\exp\underbrace{\left[-L\sum_j \sigma_j(\lambda)c_j\right]}_{\text{Narrow band feature}} \qquad (26).$$

Here $A(\lambda)$ is a factor summarizing the instrumental effect and the turbulence effect. Eq. 26 can be simplified into

$$I(\lambda) = I_o^b(\lambda)\exp\left[-L\sum_j \sigma_j(\lambda)c_j\right] \qquad (27),$$

with $I_o^b(\lambda) \equiv I_o(\lambda)\exp[\varepsilon_R(\lambda)+\varepsilon_M(\lambda)]\,A(\lambda)$ expressing the broad band feature of the measured spectrum.

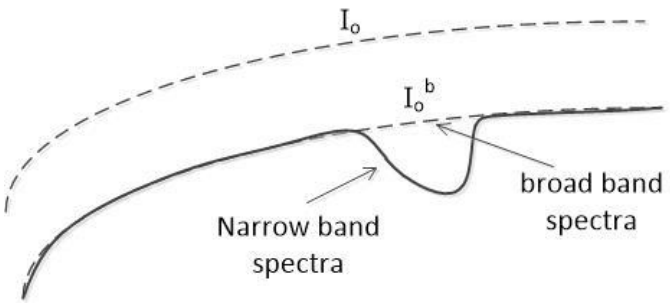

Figure 8 Principle of DOAS: Separation of broad band and narrow band features from the measured signal spectrum.

2.6.2 Typical DOAS Setup

A typical DOAS setup is shown in Fig. 9. The main components of this setup are a light source, collimating and focusing optics, a monochromator, a CCD Camera and a personal computer. The light source should have a smooth spectrum in order not to interfere with gas absorption spectrum. The intensity of the light source $I_o(\lambda)$ is transmitted through the path length L and the transmitted intensity $I(\lambda)$ is focused into the monochromator. The monochromator diffracts the transmitted light $I(\lambda)$ into a spectrum of wavelength components $I^*(\lambda)$. The diffracted spectrum is digitized by the CCD camera into intensity $I^{**}(\lambda)$ which is stored as digital data by the personal computer.

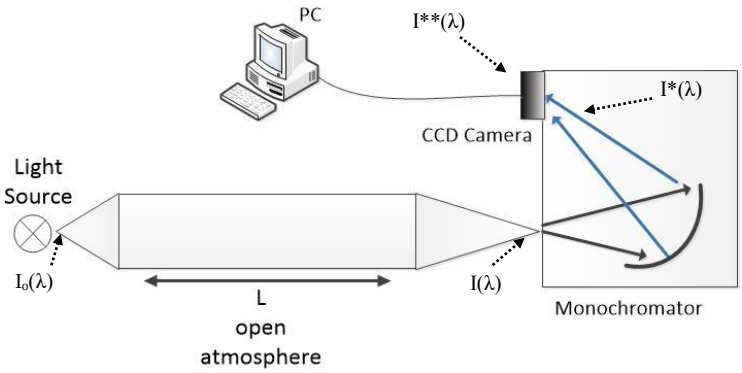

Figure 9 A schematic view of a DOAS instrument. $I_o(\lambda)$ is the intensity of the light source, $\boldsymbol{I(\lambda)}$ is the intensity of the transmitted light, $\boldsymbol{I^*(\lambda)}$ is the intensity of the diffracted light by the monochromator and the $\boldsymbol{I^{**}(\lambda)}$ is the intensity measured by the CCD camera.

2.6.3 Instrument Function of Monochromator

Due to limited resolution of a monochromator, the shape of the spectrum of the light incident on the monochromator is changed from $I(\lambda)$ to $I^*(\lambda)$. Mathematically, $I^*(\lambda)$ is equal to the convolution of $I(\lambda)$ with the instrument function of monochromator $H(\lambda)$.

$$I^*(\lambda) = \int_{-\infty}^{\infty} I(\lambda - \lambda')H(\lambda')\, d\lambda' \quad (28),$$

$H(\lambda)$ can be determined experimentally by using a light with a very narrow band compared with the resolution of the monochromator such as light emitted due to atomic transition. Atomic transitions have very narrow line emission that can be treated as delta function $\delta(\lambda)$ compared with the resolution of a typical monochromator. That is

$$I(\lambda - \lambda') \cong \delta(\lambda - \lambda') \quad (29).$$

Using this approximation into Eq. 28, then we have

$$I^*(\lambda) = \int_{-\infty}^{\infty} \delta(\lambda - \lambda')H(\lambda')\, d\lambda' \quad (30),$$

$$I^*(\lambda) = H(\lambda) \quad (31).$$

Then the measured spectrum of this narrow line emission is the monochromator's instrument function as it is illustrated in Fig. 10.

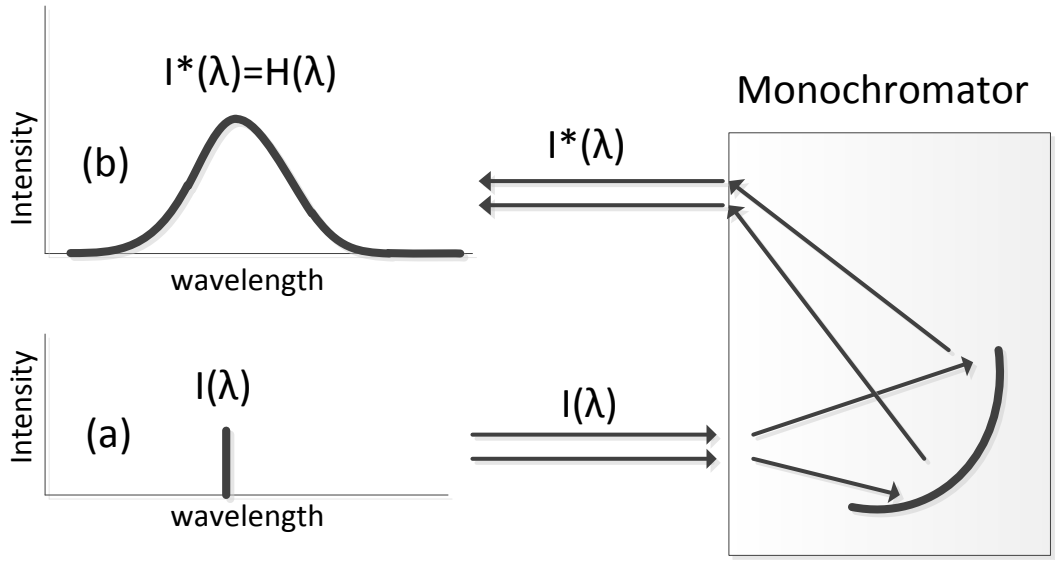

Figure 10. The monochromator instrument function H can be measured by measuring the spectrum of a narrow line emission spectrum $\boldsymbol{I(\lambda)}$ incident on the monochromator.

2.6.4 Discretization of spectrum by CCD Camera

CCD Camera detects light spectrum by counting number of photons which fall in each Camera's pixel. This pixel has certain width so its reading is the integration of light spectrum within this width. For example, the detected light intensity at pixel i, $I^{**}(i)$, is an accumulation of light intensity $I^{*}(\lambda)$ in wavelength interval from $\lambda(i-\frac{1}{2})$ to $\lambda(i+\frac{1}{2})$

$$I^{**}(i) = \int_{\lambda(i-\frac{1}{2})}^{\lambda(i+\frac{1}{2})} I^{*}(\lambda').\mathrm{d}\lambda' \qquad (32).$$

Mapping process of light spectrum into n discrete number pixel is illustrated in Fig. 11.

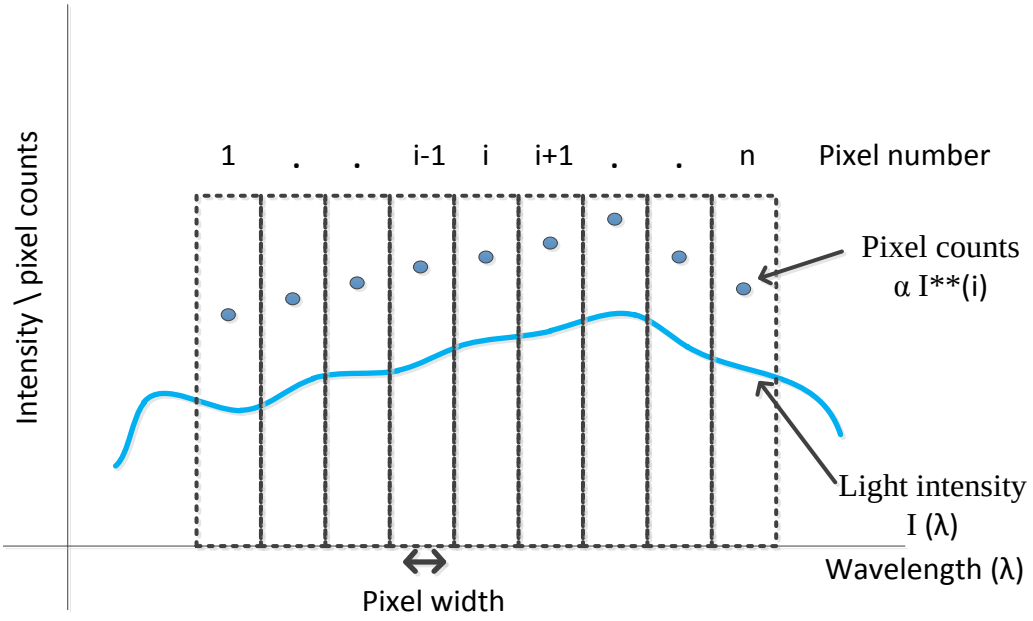

Figure 11 Mapping process of light spectrum according to CCD camera's pixels. Continuous light intensity (blue line) is integrated over a pixel width and assigned as a single value of pixel's intensity (dot).

2.6.5 Measured Light Spectrum

The light experiences absorption and scattering in the open atmosphere, then it is convolved with spectrometer instrument function and, finally, it is digitized by the CCD camera. Using equations 27, 28 and 32, these effects can be expressed mathematically as

$$I^{**}(i) = \int_{\lambda(i-\frac{1}{2})}^{\lambda(i+\frac{1}{2})} \left\{ \int_{-\infty}^{\infty} I_o^b\left(\lambda_j'' - \lambda'\right) e^{-\sigma\left(\lambda_j''-\lambda'\right)cL} H(\lambda')\, d\lambda' \right\} d\lambda'' \qquad (33).$$

2.6.6 Linear Model of Light Propagation in the Open Atmosphere

In principle, the concentration can be obtained by fitting the measured spectrum to a model described by the right hand side of Eq. 33. However, this involves doing non-linear fitting since the model is a non-linear function of the concentration. Generally, nonlinear fitting is difficult and depends on the initial conditions and may not give a unique solution. It is more convenient to work with linear models. If the light source is smooth and the

absorption is small, Eq. 33 can be approximated to a linear function of the concentration as it will be shown in the following discussion.

For a smooth light source, Eq. 33 can be approximated as:

$$I^{**}(i) \cong I_o^b(i) \int_{\lambda(i-\frac{1}{2})}^{\lambda(i+\frac{1}{2})} \left\{ \int_{-\infty}^{\infty} e^{-\sigma\left(\lambda_j'' - \lambda'\right) cL} H(\lambda')\, d\lambda' \right\} d\lambda'' \tag{34}.$$

If there is no light extinction due to absorption or scattering, then $I^{**}(i) = I_o^{**}(i)$. In this case the measured background light I_o^{**} can be written as:

$$I_o^{**}(i) \cong I_o(i) \int_{\lambda(i-\frac{1}{2})}^{\lambda(i+\frac{1}{2})} \left\{ \int_{-\infty}^{\infty} H(\lambda')\, d\lambda' \right\} d\lambda'' \tag{35}.$$

The integration of the instrument function over a range much larger than the resolution of the monochromator is by definition equal to 1. Hence,

$$\int_{-\infty}^{\infty} H(\lambda')\, d\lambda' = 1 \tag{36}.$$

Applying this to Eq. 35 leads to

$$I_o^{**}(i) = I_o(i) \int_{\lambda(i-\frac{1}{2})}^{\lambda(i+\frac{1}{2})} d\lambda'' \tag{37}.$$

Using

$$n'' \equiv \int_{\lambda(i-\frac{1}{2})}^{\lambda(i+\frac{1}{2})} d\lambda'' \tag{38},$$

leads to

$$I_o^{**}(i) = I_o(i)\, n'' \tag{39}.$$

Dividing Eq. 34 by Eq. 39 and taking the logarithm of both sides leads to

$$Ln\left[\frac{I^{**}(i)}{I_o^{**}(i)}\right] \cong Ln\left[\frac{I_o^b(i)}{I_o(i)\, n''} \int_{\lambda(i-\frac{1}{2})}^{\lambda(i+\frac{1}{2})} \left\{ \int_{-\infty}^{\infty} e^{-\sigma\left(\lambda_j'' - \lambda'\right) cL} H(\lambda')\, d\lambda' \right\} d\lambda''\right] \tag{40}.$$

Using the definition of optical density $OD(i) \equiv Ln\left[\frac{I^{**}(i)}{I_o^{**}(i)}\right]$ gives

$$OD(i) = Ln\left[\frac{I_o^b(i)}{I_o(i)\,n''}\int_{\lambda(i-\frac{1}{2})}^{\lambda(i+\frac{1}{2})}\left\{\int_{-\infty}^{\infty} e^{-\sigma(\lambda_i''-\lambda')cL}H(\lambda')\,d\lambda'\right\}d\lambda''\right] \quad (41),$$

$$OD(i) = Ln\left[\frac{I_o^b(i)}{I_o(i)}\right] + Ln\left[\frac{1}{n''}\int_{\lambda(i-\frac{1}{2})}^{\lambda(i+\frac{1}{2})}\left\{\int_{-\infty}^{\infty} e^{-\sigma(\lambda_i''-\lambda')cL}H(\lambda')\,d\lambda'\right\}d\lambda''\right] \quad (42).$$

For small concentration such that $\sigma(\lambda_i'' - \lambda')\,cL \ll 1$, as shown in Appendix A, Eq. 42 can be approximated to

$$OD(i) = Ln\left[\frac{I_o^b(i)}{I_o(i)}\right] + \frac{Lc}{\alpha}Ln\left[\frac{1}{n''}\int_{\lambda(i-\frac{1}{2})}^{\lambda(i+\frac{1}{2})}\left\{\int_{-\infty}^{\infty} e^{-\sigma(\lambda_i''-\lambda')\,\alpha}H(\lambda')\,d\lambda'\right\}d\lambda''\right] \quad (43),$$

which is a linear function of concentration. Here α is a factor to make the argument of the exponential function dimensionless. Usually the product $\sigma\alpha$ is made much smaller than 1 but large enough for the computer to handle. For example, a typical value for the NO_2 cross-section around 450 nm is 10^{-19} cm^2/ molecule an acceptable value for α is 10^{15} / cm^2 which leads to $\sigma\alpha$ of order of 10^{-4}.

The first term of Eq. 43 can be written as

$$Ln\left[\frac{I_o^b(i)}{I_o(i)}\right] = \{\varepsilon_R(i) + \varepsilon_M(i)\}.Ln[A(i)] \quad (44).$$

This is a broad band function [24] which can be modeled as a polynomial function

$$Ln\left[\frac{I_o^b(i)}{I_o(i)}\right] \cong \sum_{h=0}^{r} \mathrm{a_h}\,.(i - i_c)^{\mathrm{h}} \quad (45),$$

with i_c is center pixel of the spectral region used for evaluation.

The second term of Eq. 43 can be written as $a_s S(i)$, with

$$a_s \equiv \frac{L\,c}{\alpha} \quad (46),$$

and

$$S(i) \equiv Ln\left[\frac{1}{n''}\int_{\lambda(i-\frac{1}{2})}^{\lambda(i+\frac{1}{2})}\left\{\int_{-\infty}^{\infty} e^{-\sigma(\lambda_i''-\lambda')\,\alpha} H(\lambda')\,d\lambda'\right\}d\lambda''\right] \quad (47).$$

Hence, a_s is a scaling factor of the reference spectrum $S(i)$.

Using Eqs. 44, 45, and 47, Eq. 43 can be expressed as

$$OD(i) \cong \sum_{h=0}^{r} a_h\,(i-i_c)^{\mathrm{h}} + a_s\,S(i) \quad (48).$$

Thus the measured optical density $OD(i)$ can be described as a sum of a polynomial of order r and a reference spectrum $S(i)$ multiplied by a factor proportional to the gas concentration. In order to extract the gas concentration, we need to find the scaling factor a_s that best fits the measured $OD(i)$ profile to the right hand side of Eq. 48. The most common technique to find the best fit is to use the least square technique which will be discussed in the next section.

2.6.7 Least Square Fitting

Least square fitting is a common method to compare experimental data with theoretical models. The basic idea behind this method is to minimize the square of the difference between measured data points $y(i)$ and a model function $F(i, a_0, a_1, ..)$ where i is the independent variable and a_0, a_1, ... are the model parameters. To quantify this, one needs to minimize χ^2 which is defined as

$$\chi^2 \equiv \frac{1}{n}\sum_{i=0}^{n-1}\{y(i) - F(i, a_o, a_i, ..)\}^2 \quad (49).$$

In our case, see Eq. 48, our data points are $OD(i)$ and our model is $\sum_{h=0}^{r} a_h(i-i_c)^h + a_s.S(i)$, hence Eq. 49 becomes :

$$\chi^2 \equiv \frac{1}{n}\sum_{i=0}^{n-1}\left\{OD(i) - \left[\sum_{h=0}^{r} a_h(i-i_c)^h + a_s.S(i)\right]\right\}^2 \quad (50).$$

It can be shown that minimizing Eq. 50 with respect to the fitting parameters $a_0, \dots, a_r, a_s$ leads to [26]:

$$\vec{a} = [\boldsymbol{X}^T\boldsymbol{X}]^{-1}\boldsymbol{X}^T\overrightarrow{OD} \quad (51),$$

where

$$\vec{a} \equiv \begin{bmatrix} a_0 \\ a_1 \\ .. \\ a_r \\ a_s \end{bmatrix} \quad (52\text{-a}),$$

$$\boldsymbol{X} \equiv \overbrace{\begin{bmatrix} 1 & (-i_c)^1 & (-i_c)^2 & . & (-i_c)^r & S(0) \\ 1 & (1-i_c)^1 & (1-i_c)^2 & . & (1-i_c)^2 & S(1) \\ . & . & . & . & . & . \\ . & . & . & . & . & . \\ 1 & (n-1-i_c)^1 & (n-1-i_c)^2 & . & (n-1-i_c)^2 & S(n-1) \end{bmatrix}}^{r+2} \Bigg\}n \quad (52\text{-b}),$$

and

$$\overrightarrow{OD} \equiv \begin{bmatrix} OD(0) \\ OD(1) \\ .. \\ OD(n-2) \\ OD(n-1) \end{bmatrix} \quad (52\text{-c}).$$

The vector $\vec{a}$ is the parameters vector, the vector $\overrightarrow{OD}$ is the measured optical density vector, $\boldsymbol{X}^T$ is the transpose matrix of the $\boldsymbol{X}$ matrix.

The uncertainty Δa_j in the parameters a_j, where $j = 0,1, \dots, r, and\ s$ is given by [27]:

$$\Delta a_j = \sqrt{\Theta_{jj}} \quad (53),$$

where

$$\Theta = \hat{\boldsymbol{\sigma}}^2[\boldsymbol{X}^T\boldsymbol{X}]^{-1} \quad (54),$$

where

$$\hat{\boldsymbol{\sigma}}^2 = (n-m)^{-1}[\overrightarrow{OD} - \boldsymbol{X}\vec{a}]^T\left[\overrightarrow{OD} - \boldsymbol{X}\vec{a}\right] \quad (55).$$

Finally, the concentration of the gas could be determined from

$$c = \frac{a_s \alpha}{L} \quad (56).$$

The concentration can be expressed in part per million of a mixture of air molecules by using the fact that the number of air molecules N per unit volume V is related to the pressure P and absolute temperature T by the ideal gas law $\frac{N}{V} = \frac{P}{kT}$, where k is the Boltzmann constant. Hence, the concentration expressed in the part per million (ppm) unit is :

$$c = \frac{a_s.\alpha}{L} \times \frac{k.T}{P} \times 10^6 \ (ppm) \quad (57),$$

$$\Delta c = \frac{\Delta a_s.\alpha}{L} \times \frac{k.T}{P} \times 10^6 \ (ppm) \quad (58).$$

2.7 Corrections of the Measured Spectrum

Before analyzing, the measured spectrum should be corrected for electronic offset, dark current, stray light.

2.7.1 Electronic Offset

To avoid the non-linearity of the analog-to-digital converts at very low voltages, an offset voltage is added to the voltages produced by the pixels of a CCD camera. Even if there is no light incident on the camera and with the shortest possible integration time, the CCD camera registers some counts corresponding to this offset voltage. The offset can be

determined by setting a very shot integration time while no light is entering the CCD camera.

2.7.2 Dark Current

The dark current is produced by thermally excited electrons in the CCD camera electronic system. The dark current counts can be easily measured by recording a spectrum in a dark condition using the same integration time as that of the experiment. This should be subtracted from the real measured spectrum.

2.7.3 Stray Light

Stray light may be produced as a result of a higher-order diffraction by the grating. This light could reach detector then disturb the original signal. The correction of the stray light can be done by fitting an additional polynomial in spectral analysis.

2.8 Determination of the Reference Spectrum

There are two methods to determine the reference spectrum $S(i)$:

1) **Measurement of the reference spectrum using known gas concentration.**

   Measurement of the reference spectrum using a gas sample with a known concentration is the most direct and often the most successful approach to obtain the correct reference spectrum $S(i)$ since the convolution with the instrument function is performed through the measurement.

2) **Calculation of the reference spectrum using a high resolution gas absorption cross-section spectrum.**

   The reference spectrum can also be calculated using a high resolution NO_2 absorption cross-section spectrum $\sigma_{ref}(\lambda)$ using Eq. 47

$$S(i) = Ln\left[\frac{1}{n''}\sum_{j=js}^{je}\int_{-\Delta\lambda'}^{\Delta\lambda'} e^{-\sigma\left(\lambda_j^{ref}-\lambda'\right)^{\alpha}} H(\lambda')\, d\lambda'\right] \quad (59),$$

where

$$\lambda_{js}^{reff} = \lambda\left(i - \frac{1}{2}\right) \quad (60),$$

$$\lambda_{je}^{reff} = \lambda\left(i + \frac{1}{2}\right) \quad (61),$$

and n'' is number of reference data between λ_{js}^{reff} and λ_{je}^{reff}

$$n'' = \sum_{\lambda_{js}^{reff}}^{\lambda_{je}^{reff}} 1 \quad (62).$$

2.9 DOAS Method Algorithm

The steps of DOAS methods described in previous sections are summarized in Fig. 12.

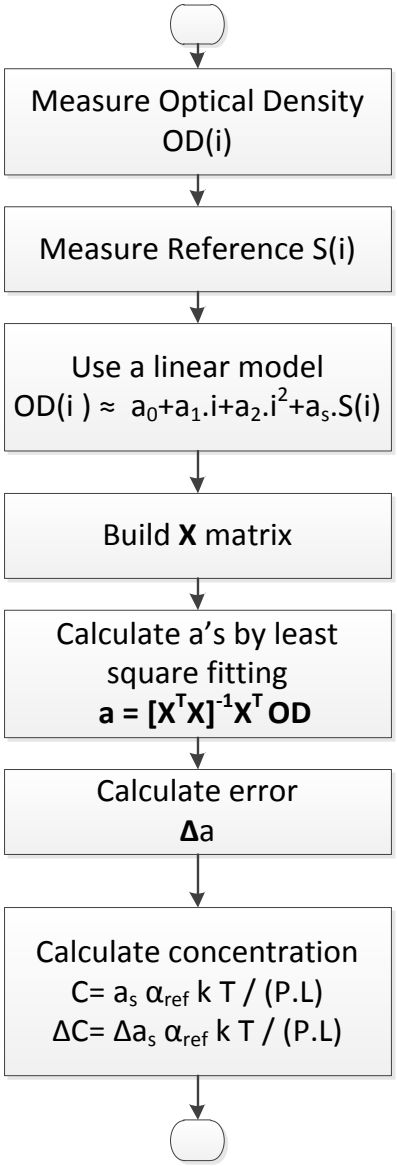

Figure 12 Flowchart of DOAS method

CHAPTER 3

EXPERIMENTAL SETUP AND PROCEDURE

In this section, the experimental setup and procedure are discussed.

3.1 Experimental Setup

3.1.1 DOAS Experiment Setup

A diagram and a picture of the experimental setup are shown in Fig.13 and Fig. 14, respectively. Two pressurized gas cylinders of highly purified N_2 gas and NO_2/N_2 gas mixture, see Fig. 15, are connected to a 15.5-cm long cell using ¼" Teflon tubes and two Swagelok valves which are used to further control the mixing gas ratios. The cell is made of aluminum alloy with an outer diameter of 2.5 cm and inner diameter of 1.0 cm. 2-mm thick BK7 windows are used to close the ends of the cell. The windows are purposely tilted with respect to the axis of the cell to eliminate light interference from the surfaces of the windows. The inlet line of the cell is connected to the gas cylinders while its outlet line is connected to an exhaust line. The light from a commercial white LED, see Fig.16, is collimated into the cell by an iris diaphragm and a double concave lens of a focal length of 7.5 cm and a diameter of 2.5 cm. The collimated light beam is made small enough that no light hit the side of the cell. Another double concave lens is used to focus the light beam into the entrance of a Horiba SPEX500M monochromator, see Fig. 17. The entrance width is adjusted to be about 6 μm. A Thorlab LC1-USB line CCD Camera, see Fig.18, is attached to the monochromator to detect the diffracted light. The camera has 3000 pixels each of which has a width of 7 μm and a length of 200 μm. The spectrum digitized by the

line CCD Camera is transferred to a personal computer using a LabView code written locally for this purpose. An Orion LX Weather Station is used to measure the room temperature and pressure.

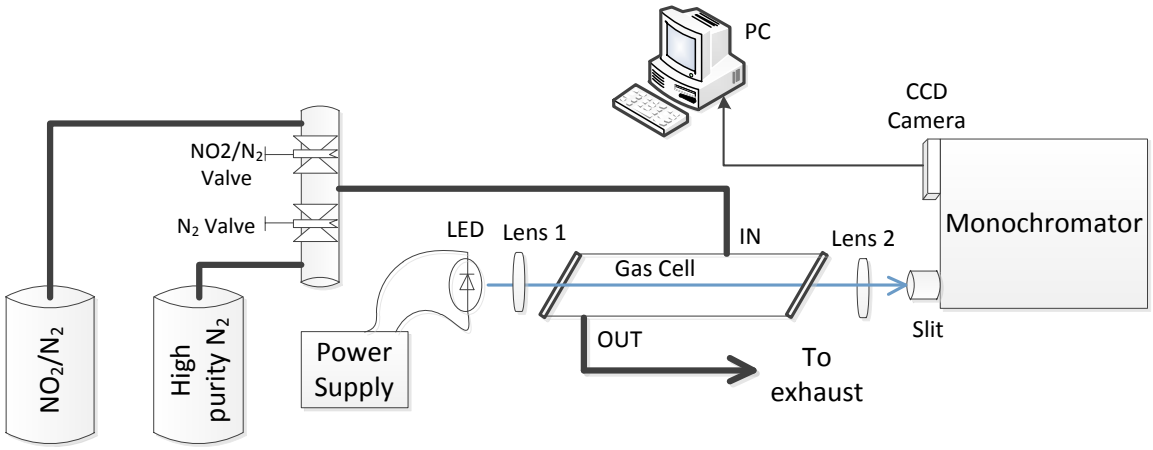

Figure 13 A diagram of the DOAS experimental setup

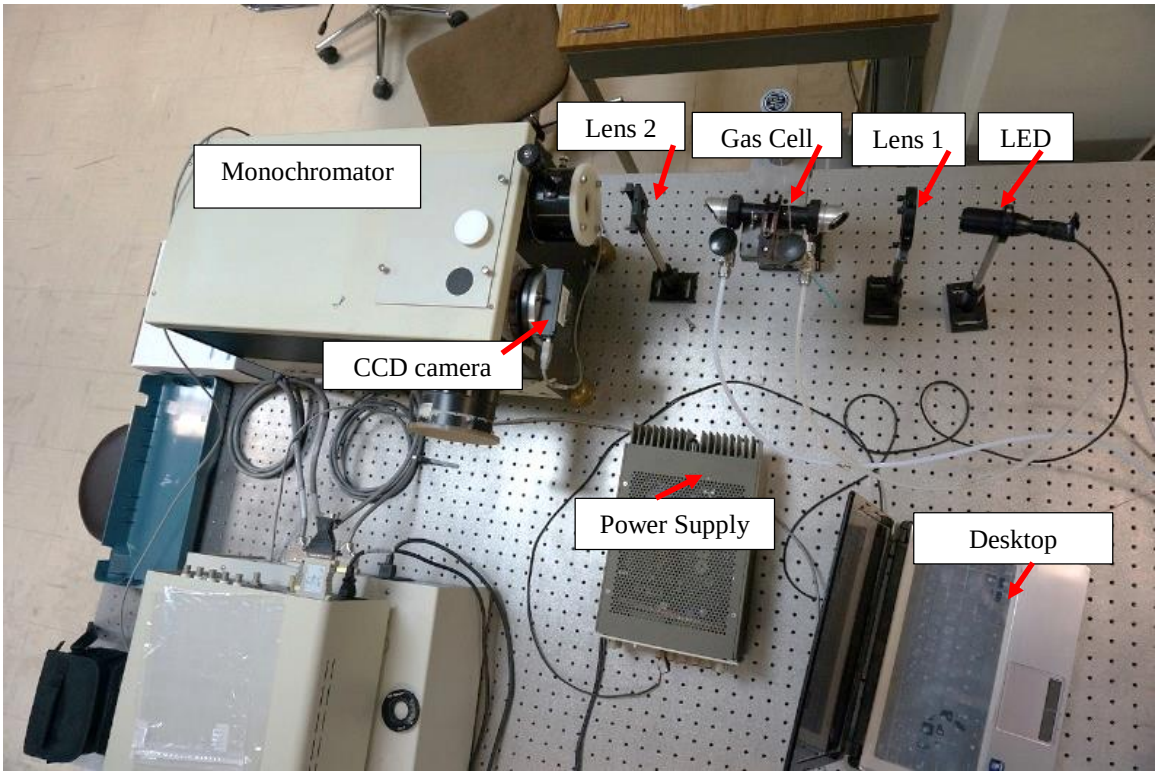

Figure 14. A top view picture of the DOAS experimental setup.

Figure 15 NO_2/N_2 gas cylinders under an exhaust hood

Figure 16 A commercial white LED used as a light source

Figure 17. A Horriba SPEX500M monochromator with a 0.013-nm resolution

Figure 18 A Thorlab LC-1 line CCD camera.

3.1.2 Calibration of the SPEX500M Monochromator

A monochromator wavelength calibration is the process of establishing a relationship between the diffracted light wavelength and the pixel numbers of the line CCD camera. Fig.19 show a diagram of the setup used in calibrating the Horriba SPEX500M monochromator. The light from a krypton discharge lamp is focused by a lens into the entrance of the SPEX500M monochromator which is set at 450.00 nm. The Krypton lamp

has several lines in the spectral region of interest [28]: 436.26 nm, 437.61 nm, 445.39 nm, 446.37 nm and 450.24 nm.

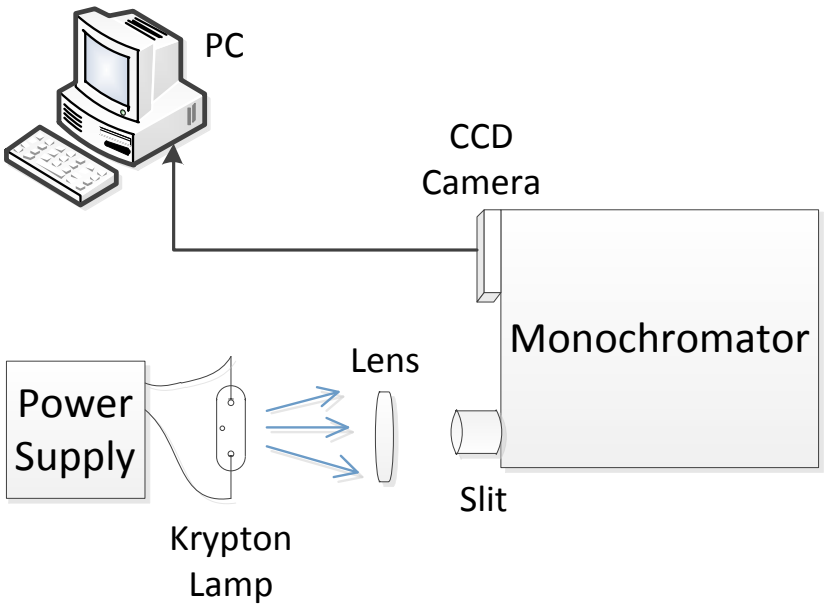

Figure 19 A diagram of the experimental setup used in the SPEX500M monochromator calibration

3.2 DOAS Experimental Procedure and Experimental setup stability

In a DOAS measurement, two spectra are needed: a background spectrum and a signal spectrum. The background spectrum $I_o(\lambda)$ is the spectrum detected when no NO_2 gas is present in the cell and only a highly purified N_2 gas is admitted into the cell. While the signal spectrum $I(\lambda)$ is the spectrum detected when some NO_2/N_2 is admitted into the cell. A pure N_2 gas is used since it does not have absorption interfering with the NO_2 absorption in the spectral range 435 – 465 nm. N_2 gas has dominant absorption at $\lambda < 200\ nm$ [28].

Two NO_2 gas concentrations are used. A concentration of 206 ppm is used for measuring the reference spectrum $S(i)$, see sec 2.8. A concentration of 2.6 ppm is used for testing the accuracy of the DOAS method and to determine the detection limit.

It is observed that when an NO_2 gas mixture is trapped in the cell, the absorption signal decreases with time because, probably, the NO_2 molecules adsorb on the wall of the cell. To eliminate this effect, the NO_2 gas mixture must be flowing into the cell. Typically, a 5-minute waiting time is allowed between measuring the background spectrum and the signal spectrum to ensure that the steady state condition is reached.

A LabVIEW [29] code is developed for recording measured spectra from the CCD Camera along with the room temperature and pressure as well as the date and time. Table 3 shows the format written by the LabVIEW code. The integration time of the CCD line camera is set to 25 ms and each measured spectrum is an average of 1000 spectra. Thus each spectrum takes about 25 s to collect and the total time for measuring a set of a background spectrum and a signal spectrum is about 6 minutes.

Table 3 File format of experimental data

Column 1	Column 2	Column 3	Column 4	Column 5
Pixel Location	Intensity	Room temperature	Room Pressure	Date and Time

Before being able to perform reliable DOAS measurements, the stability of the experimental setup needs to be checked.

The stability of the experimental setup is tested by taking 200 different spectra over a 4-hour period under the same experimental conditions. The purpose of these measurements is to determine the drift of the intensity recorded by each pixel over time. This measurement is important since each set of DOAS measurement takes about 6 minutes. The drift must be very small during this time scale.

CHAPTER 4

RESULTS AND DISCUSSION

This chapter discusses the experimental results. First, we present the results for the wavelength calibration of the monochromator and we also present the measured monochromator instrument function $H(\lambda)$. Then, we discuss the stability obtained for the experimental setup. Finally, we show detailed steps for extracting NO_2 gas concentration using DOAS method and discuss the detection limit of our setup.

4.1 SPEX500M Wavelength Calibration

Wavelength calibration of the SPEX500M monochromator is done using six emission atomic lines from a krypton discharge lamp. The six lines are clearly detected within the pixel range from pixel number 323 to 1510 as shown in Fig.20. The location of the peak of an emission line is found by fitting its spectrum to a Gaussian function as shown in Fig. 22. The locations of the peaks on the CCD camera and their corresponding wavelength are listed in Table 4. To calibrate the monochromator, a linear relation between the locations of the peaks measured in pixels and the corresponding wavelengths should be obtained, namely,

$$\lambda(i) = b_0 + b_1 i \qquad (63).$$

where i is the pixel number b_0, and b_1 are fitting parameters. Although, this fitting can be done with many plotting programs, such as Excel, the fitting has been done with the method discussed in Sec. 2.6.7.

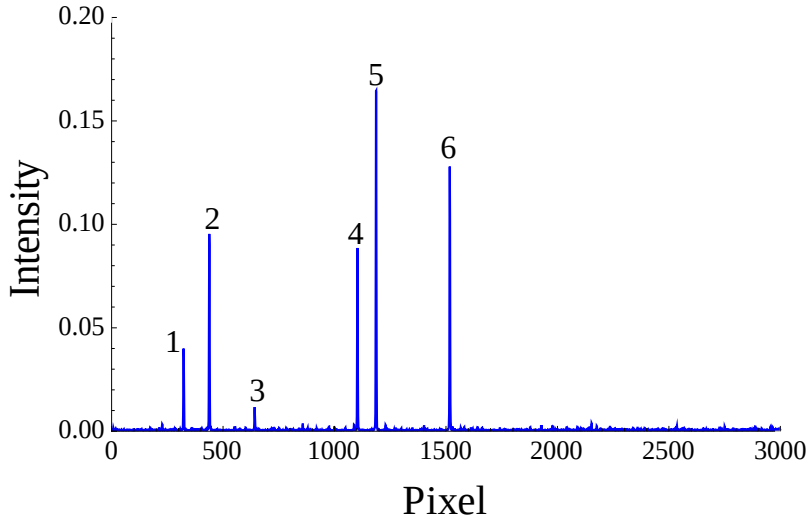

Figure 20 Six lines of Krypton lines detected by SPEX500M Horiba

Table 4. Krypton lines peak locations on the CCD line camera and their corresponding wavelengths

No	peak location i_l(pixel)	Wavelength λ (nm)
1	323.4	436.26
2	438.4	437.61
3	642.0	440.00
4	1102.9	445.39
5	1186.5	446.37
6	1517.2	450.24

Let the data vector or the krypton wavelengths vector be $\vec{\lambda}_{kr}$

$$\vec{\lambda}_{kr} = \begin{bmatrix} 436.26 \\ 436.61 \\ 440.00 \\ 445.39 \\ 446.37 \\ 450.24 \end{bmatrix} \quad (64).$$

The X matrix is

$$\boldsymbol{X} \equiv \begin{bmatrix} 1 & (323.4 - 1500) \\ 1 & (438.4 - 1500) \\ 1 & (642.0 - 1500) \\ 1 & (1102.9 - 1500) \\ 1 & (1186.5 - 1500) \\ 1 & (1517.2 - 1500) \end{bmatrix} \quad (65),$$

where $i_c = 1500$ is the central pixel since the LC1-USB CCD camera has 3000 pixels. Then, the parameter vector $\vec{b}$ is given by

$$\vec{b} \equiv \begin{bmatrix} b_0 \\ b_1 \end{bmatrix} = [\boldsymbol{X}^T \boldsymbol{X}]^{-1} \boldsymbol{X}^T \vec{\lambda}_{kr} = \begin{bmatrix} 432.477\ nm \\ 0.0117\ \frac{nm}{pixel} \end{bmatrix} \quad (66).$$

Hence the calibration relationship is:

$$\lambda(i) = 432.477 + 0.011708\ i \quad (67),$$

the error in b_0 is 0.003 nm and the error in b_1 is 0.000003 nm/pixel. The calibration relationship and data points are shown in Fig. 21.

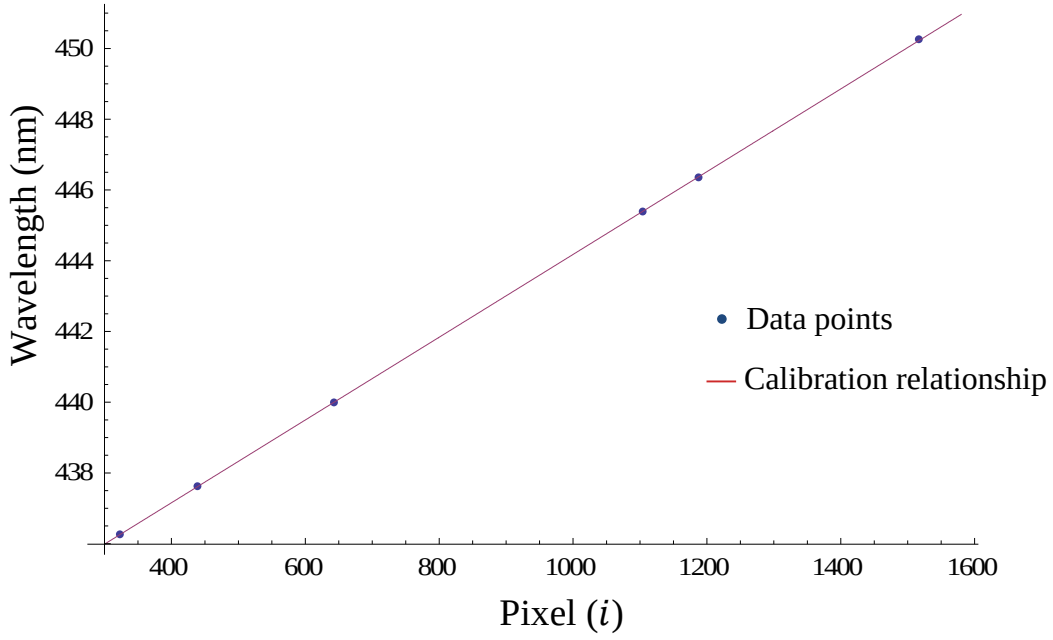

Figure 21 Calibration relationship of wavelength with respect to pixel number.

4.2 Instrument Function

The shape of a krypton emission line measured by the monochromator is proportional to the monochromator instrument function. The shape of the line fits very well to a Gaussian function $G(i) = A\exp[-\frac{(i-i_l)^2}{2\,w^2}]$, where A is the high of the peak, i_l is the peak location and pixels, and w is the resolution measured in pixels. The instrument function is $H(i) = \frac{1}{w\sqrt{2\pi}}\exp[-\frac{(i-i_l)^2}{2\,w^2}]$, the height of the function is adjusted such that the area under the function is one.

Fig.22 shows the 446.37 nm krypton emission line fitted to a Gaussian function. For this line $A = 0.176$, $w = 1.3$ and $i_c = 1186.5$. Based on these parameters, it can be concluded that the resolution of the SPEX500M monochromator is 1.3 pixel. According to Eq. 67, one pixel is equivalent to 0.0117 nm so a resolution of 1.3 pixel is equivalent to a resolution of 0.015 nm.

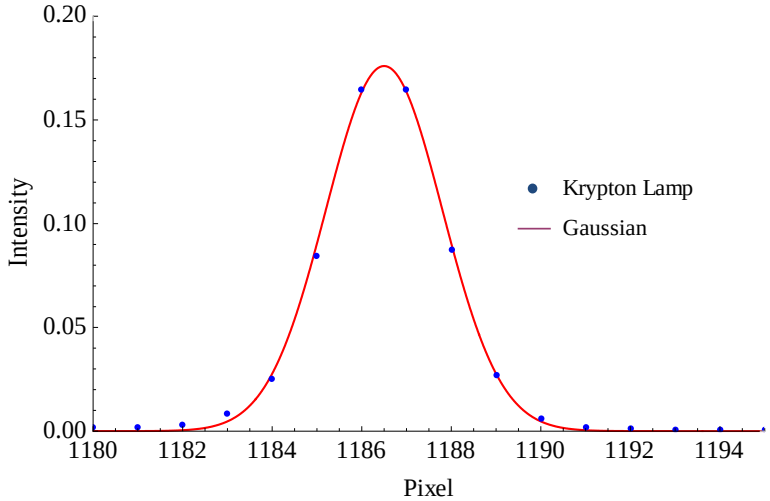

Figure 22 Fitting of the 446.37 nm krypton line (blue dots) with a Gaussian function (red line).

4.3 Instrumental Setup Stability

Stability of the DOAS setup was tested over a 200-minute period by recording an averaged spectrum of the LED emission every minute. Each averaged spectrum is a result of averaging 1000 spectra each of which takes 25 ms to collect and hence the averaged spectrum takes about 25 s to collect. The average of the 200 averaged spectra $\bar{I}(\lambda)$ is shown in Fig.23. The standard deviation $\delta(\lambda)$ at each wavelength is

$$\delta(\lambda) = \sqrt{\sum_{r=1}^{h} \frac{\{I_r(\lambda) - \bar{I}(\lambda)\}^2}{h^2}} \qquad (68),$$

where I_r is the averaged spectrum r and $h = 200$ is the number of averaged spectra. The standard deviation is a measure of uncertainty. Fig. 24 shows the relative standard deviation $\frac{\delta(\lambda)}{I(\lambda,0)}$ as a function of wavelength. It can be seen the relative uncertainty in general is small and it is smaller of higher intensities.

Fig. 25 shows the evolution of relative intensities $\frac{I(\lambda,t)}{I(\lambda,0)}$) at three different wavelengths $\lambda = 438.33\,, 450.00\ and\ 461.67\ nm$ as a function of time. The drift in the intensities over 200 minutes is within 0.6% which is quite small for the purpose of our study. Also the variation in the intensities at these wavelengths is correlated. In the first 50 minutes, all of intensities are decreasing together, and then in the next 20 minutes they are increasing together.

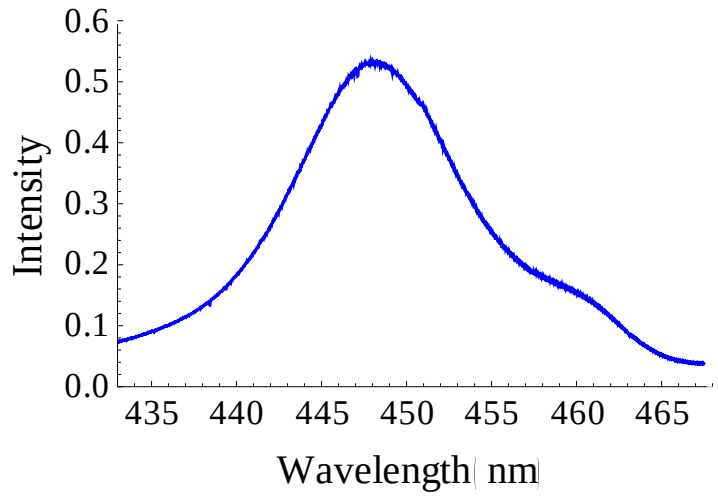

Figure 23 Average measured spectrum $\bar{I}(\lambda)$ from 200 measurements using the DOAS setup.

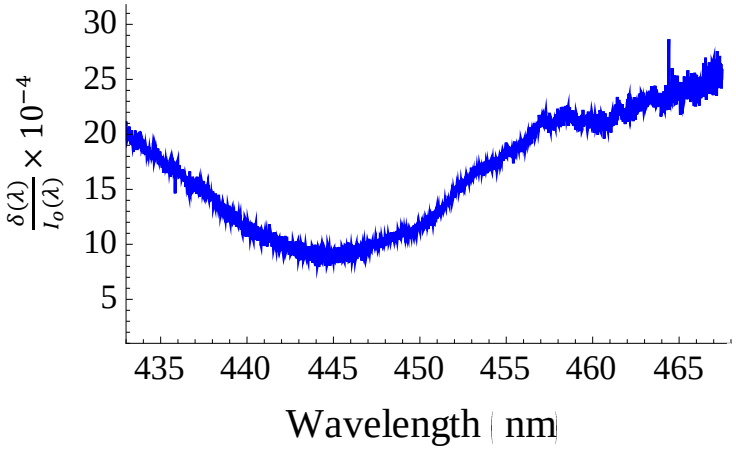

Figure 24 Relative uncertainty $\frac{\delta(\lambda)}{\bar{I}(\lambda)}$ calculated from standard deviation of 200 measurement.

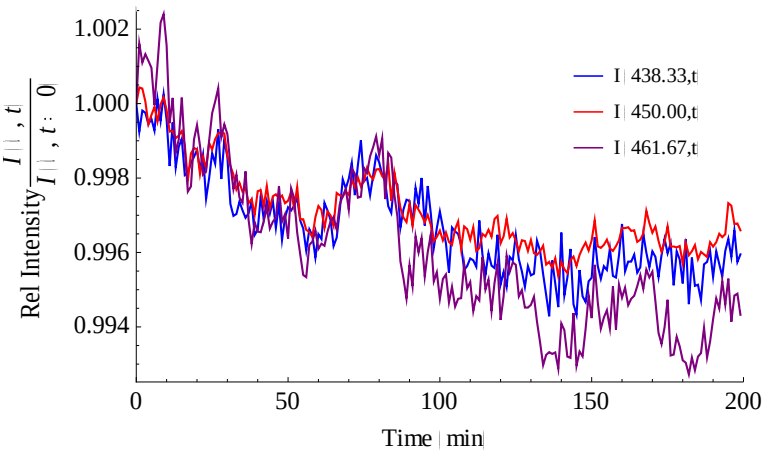

Figure 25 Evolution of relative intensities $\boldsymbol{I(\lambda, t)\ /\ I(\lambda, t = 0)}$. at λ = 438, 450 and 461.67 nm as a function of time.

Fluctuation of the measurement system should not create a spectrum similar to the NO_2 absorption spectrum in order to avoid misleading calculations of the gas concentration. To test this similarity, we calculate the optical density from two different averaged spectra

$$OD_{noise}(\lambda) = Ln\left[\frac{I_1(\lambda)}{I_2(\lambda)}\right] \quad (69),$$

then compare it with the optical density of NO_2 absorption spectrum at certain column concentration $\alpha \approx 10^{16}\ molecule/cm^2$ which corresponds to 26.12 ppm for our cell.

$$OD_{NO_2}(\lambda) = -\sigma.\alpha \quad (70).$$

These two optical densities are plotted in Fig. 26. From this figure we can conclude that there is no significant NO_2 spectrum within the noise caused by the setup.

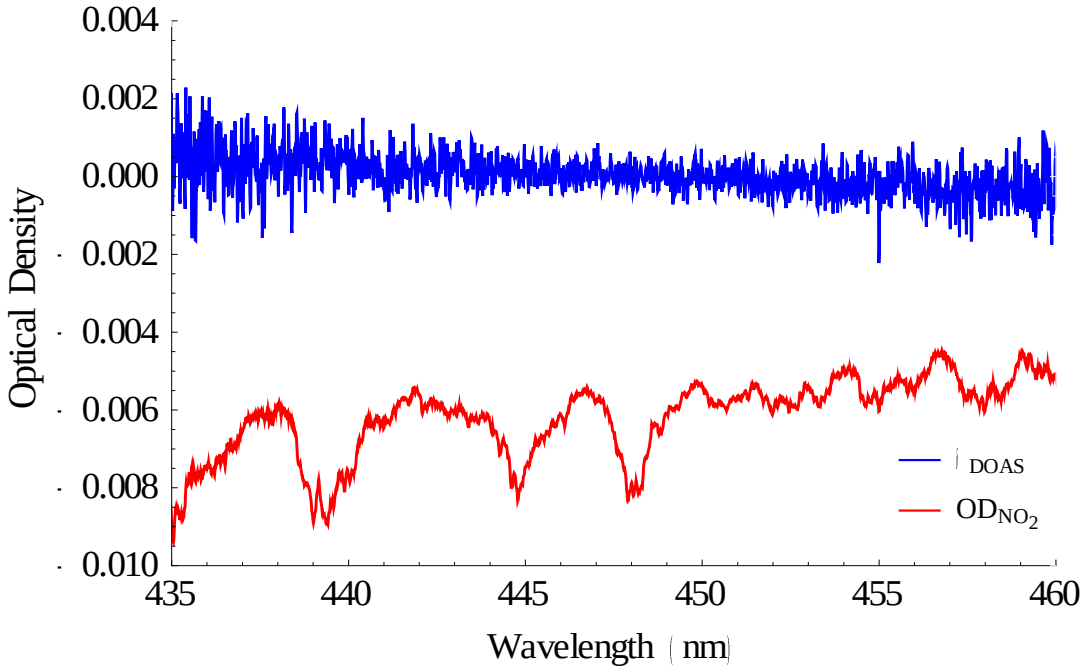

Figure 26 Comparison of two optical densities: the optical density calculated by two averaged spectra with no NO_2 in the cell and the optical density of NO_2 with a column density $\boldsymbol{\alpha = 10^{16}\ molecule/cm^2}$ that corresponds to 26.12 ppm for the length of our cell.

4.4 DOAS Analysis

In DOAS analysis gas concentration is extracted from the fitting parameters of a measured optical density spectrum to a gas reference absorption spectrum summed to a polynomial function. The polynomial function in this analysis is used to describe the low frequency profile of the measured optical density spectrum while the reference spectrum describes the high frequency profile.

To check the accuracy of the setup, two different concentrations of NO_2 are measured: 206 ppm and 2.6 ppm. Fig. 27 shows a flow chart of the steps taken to

check the accuracy. The gas reference absorption spectrum can be determined either by measuring an absorption spectrum of a known gas concentration using the experimental setup or by calculating the absorption spectrum corresponding to the resolution of the experimental setup from a higher resolution cross-section spectrum. The measured reference spectrum is denoted by $S_{mea}(\lambda)$ while the calculated reference spectrum is denoted by $S_{cal}(\lambda)$. For the 206 ppm concentration measurement, where the concentration is relatively high, a calculated spectrum is used as the reference spectrum. This measurement is used to confirm the accuracy of the concentration quoted by the gas cylinder supplier. For the 2.6 ppm concentration measurement, where the concentration is low and the optical density is near the noise level, the measured spectrum obtained from the 206 ppm concentration measurement is used as the reference spectrum. In this case, the measured reference spectrum is used rather than the calculated one to avoid errors that might have been introduced during the convolution when calculating the reference spectrum. The accuracy of our setup can be quantified by calculating the deviation of the 2.6 ppm concentration measurement and the concentration provided by the gas cylinder supplier. The following subsections describes the steps shown in Fig. 27 in more details.

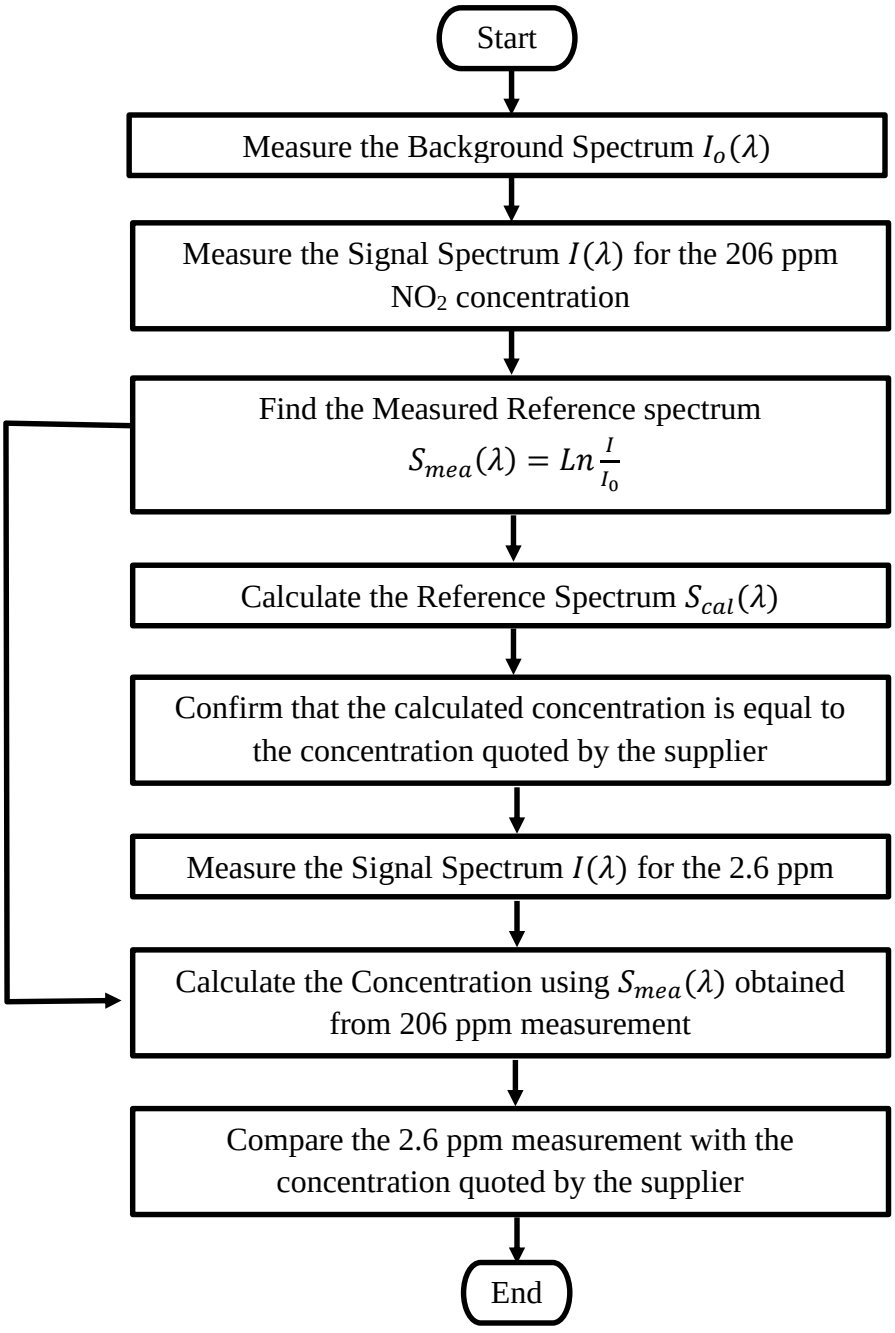

Figure 27 Flowchart showing the steps taken to check the accuracy of the setup.

4.4.1 Measured Reference Spectrum $S_{mea}(\lambda)$

The measured reference spectrum $S_{mea}(\lambda)$ is more direct and often more accurate than the calculated reference spectrum. In this work, the measured reference spectrum $S_{mea}(\lambda)$ is found from the absorption by an NO_2 gas with a concentration of 206 ppm:

$$S_{mea}(\lambda) = Ln\left[\frac{I_{206}(\lambda)}{I_o(\lambda)}\right] \quad (71).$$

The background spectrum $I_o(\lambda)$ and signal spectrum $I_{206}(\lambda)$ are shown in Fig. 28 and the measured reference spectrum $S_{mea}(\lambda)$ is shown in Fig. 29.

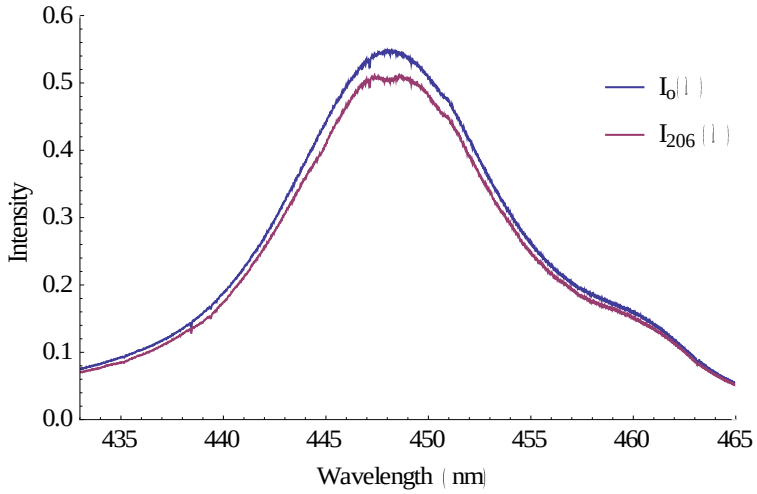

Figure 28 The background spectrum $\boldsymbol{I_o(\lambda)}$ (blue line) measured by admitting a pure N_2 gas into the gas cell and the signal spectrum $\boldsymbol{I_{206}(\lambda)}$ (red line) is measured by admitting a 206 ppm NO_2 gas into the cell.

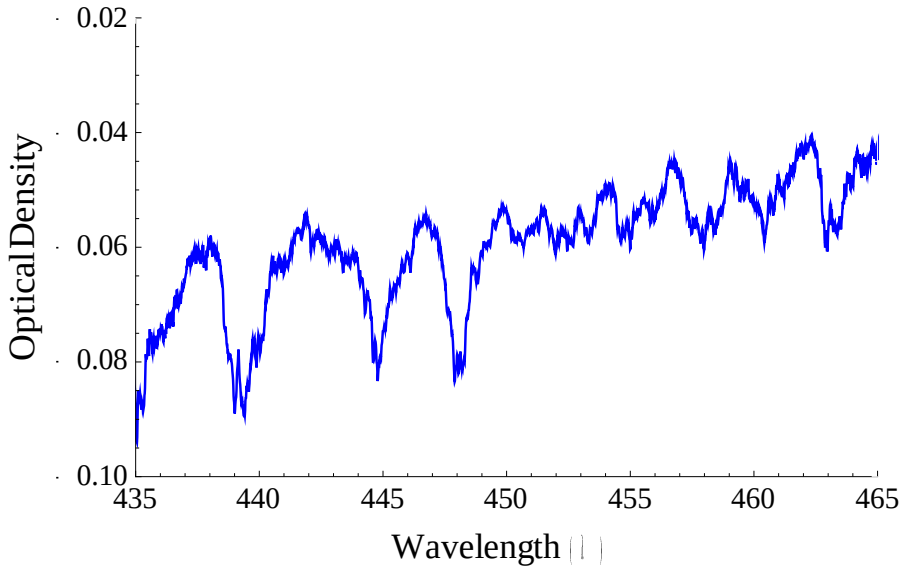

Figure 29 The measured reference $\boldsymbol{S_{mea}(\lambda)}$ obtained from absorption measurement of a 206 ppm NO_2 gas.

4.4.2 Calculated Reference Spectrum $\boldsymbol{S_{cal}(\lambda)}$

Fig. 30 shows the calculated reference spectrum $S_{cal}(\lambda)$ calculated from:

$$S_{cal}(\lambda_i) = Ln\left[\frac{1}{n''}\sum_{j=js}^{je}\int_{-\Delta\lambda'}^{\Delta\lambda'} e^{-\sigma\left(\lambda_j^{ref}-\lambda'\right)\alpha} H(\lambda')\, d\lambda'\right] \quad (72),$$

with

$$n'' = \sum_{j=j_s}^{j_e} 1 \quad (73).$$

Here $\sigma(\lambda)$ is the high resolution NO_2 cross-section retrieved from reference [12] and α is set to $10^{16}\ molecule/cm^2$ which is equivalent to an absorption from an NO_2 gas with a concentration of 26.1 ppm over a length of 15.5 cm at a temperature of 22° C and a pressure of 1.01×10^5 Pa.

Eq. 72 is derived from Eq. 47. In Eq. 47, the reference cross section spectrum is assumed to be a continuous function of wavelength, while in Eq. 72, the reference cross section spectrum is a discrete function of wavelength.

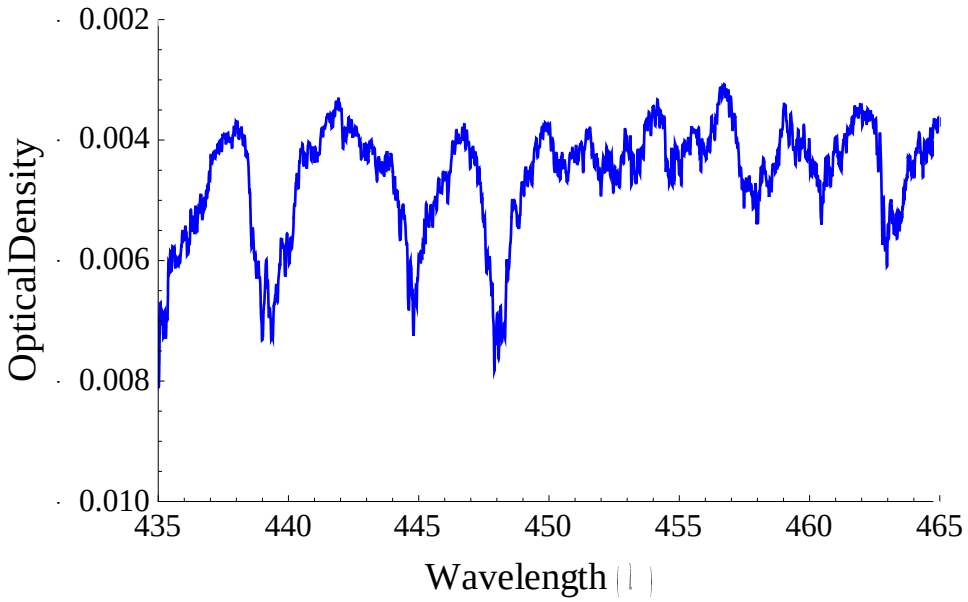

Figure 30 The calculated reference $\boldsymbol{S_{cal}(\lambda)}$ which is equivalent to the optical density from an NO_2 gas with a concentration of 26.1 ppm over a length of 15.5 cm.

4.4.3 Concentration Calculation Using Calculated Reference $\boldsymbol{S_{cal}(\lambda)}$

The concentration of the 206 ppm NO_2 gas can be extracted by fitting the measured optical density, which is called the measured reference $S_{mea}(\lambda)$, to the calculated reference $S_{cal}(\lambda)$ and a 2nd order polynomial function $P(\lambda) = \sum_{r=0}^{2} a_r \, (i - i_c)^{\,r}$

$$OD(\lambda) \equiv S_{mea}(\lambda) \cong a_s S_{cal}(\lambda) + \sum_{r=0}^{2} a_r \, (i - i_c)^{\,r} \qquad (74),$$

here a_s and $a_r's$ are the fitting parameters. The concentration is proportional to the scaling factor a_s. According to section 2.6.7 and using a 2nd order polynomial function, the X matrix is:

$$\boldsymbol{X} = \begin{bmatrix} 1 & (-1500)^1 & (-1500)^2 & S_{cal}(0) \\ 1 & (1-1500)^1 & (1-1500)^2 & S_{cal}(1) \\ . & . & . & . \\ . & . & . & . \\ 1 & (2999-1500)^1 & (2999-1500)^2 & S_{cal}(2999) \end{bmatrix} \quad (75),$$

The optical density vector $\overrightarrow{OD} = \begin{bmatrix} OD(0) \\ OD(1) \\ . \\ . \\ OD(2999) \end{bmatrix}$, and the parameter vector $\vec{a} \equiv \begin{bmatrix} a_o \\ a_1 \\ a_2 \\ a_s \end{bmatrix}$.

The fitting parameters can be calculated from

$$\vec{a} = [\boldsymbol{X}^T\boldsymbol{X}]^{-1}\boldsymbol{X}^T\overrightarrow{OD} \quad (76),$$

and their uncertainties are calculated from $\Delta a_j = \sqrt{\Theta_{jj}}$, with Θ_{jj} is calculated from Eq.54.

The fitting parameters from this calculation and their uncertainties are listed in Table 5 and the fitting results are shown in Fig. 31. The components of the fitted 2nd order polynomial function are shown in Fig. 32.

Table 5 The fitting parameters calculated using the reference $\mathbf{S_{cal}(\lambda)}$ for the 206 NO_2 gas sample.

Fitting parameter	Value	Uncertainty
a_s	7.9	0.03
a_0	-0.02	0.0001
a_1	6.5×10^{-6}	8.3×10^{-7}
a_2	1.2×10^{-9}	4.9×10^{-11}

The concentration of NO_2 gas at room temperature $T = 293\,K$ and room pressure $P = 101\,kPa$ can be calculated via Eq. 57:

$$c_{NO_2} = \frac{a_s\,\alpha}{L} \times \frac{kT}{P} \times 10^6 \quad (77),$$

$$c_{NO_2} = \frac{7.9 \times 10^{16}}{15.5} \times \frac{1}{2.475 \times 10^{19}} \times 10^6 \quad (78),$$

$$c_{NO_2} = 205.6 \text{ ppm} \quad (79).$$

And the uncertainty in the concentration can be calculated via Eq. 58:

$$\Delta c_{NO_2} = \frac{\Delta a_s \, \alpha}{L} \times \frac{kT}{P} \times 10^6 \quad (80),$$

$$\Delta c_{NO_2} = \frac{0.03 \times 10^{16}}{15.5} \times \frac{1}{2.475 \times 10^{19}} \times 10^6 \quad (81),$$

$$\Delta c_{NO_2} = 0.8 \text{ ppm} \quad (82).$$

This is an interesting result since our prediction is only deviated by 0.4 % from the quoted value (206 ppm) by the gas cylinder supplier. Here, we assume the length, the temperature, and the pressure are known to a much better accuracy than 0.4%. Moreover, the correlation between $a_s S_{cal}(\lambda)$ and $a_s S_{cal}(\lambda) + Residu$ is 0.992 which indicates an excellent fit to the model given by the right hand side of Eq. 74

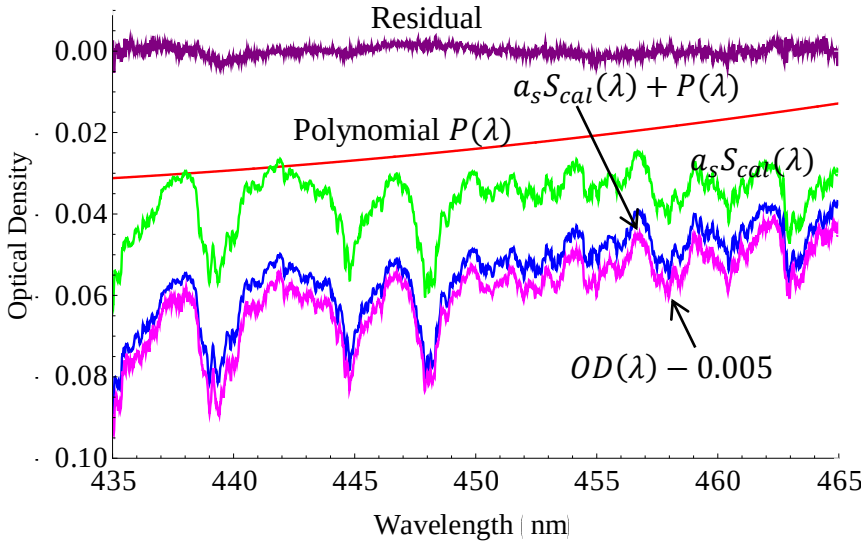

Figure 31 The measured optical density, the scaled calculated reference $\boldsymbol{a_s S_{cal}}$, the polynomial function $\boldsymbol{P(\lambda) = a_0 + a_1\lambda + a_2\lambda^2}$, and the residual. The measured optical density is shifted by -0.005 for clarity purpose.

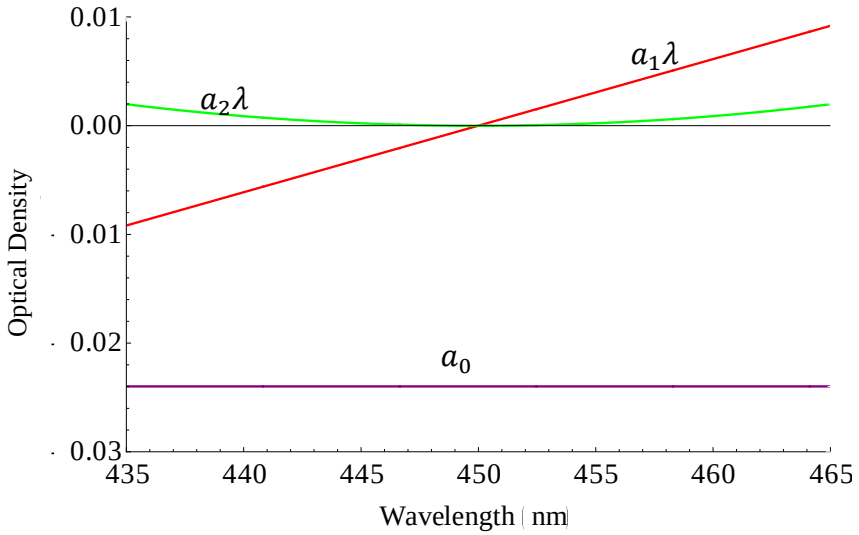

Figure 32 The components of the fitting polynomial function which is used for eliminating broad band profile in measured optical density.

4.4.4 Impact of wavelength shifting of the measured optical density and the calculated reference spectrum

A small shift in wavelength may occur due to the calibration process of the monochromator resulting in a shift in wavelength between the measured optical density and the calculated reference spectrum. To study the impact of this possible shift, the wavelength of the measured optical density is shifted by $\Delta\lambda$ with respect to the calculated reference spectrum then the fitting parameters are found according to Eq. 76. If the correlation between $a_s\, S_{cal}(\lambda)$ and $S_{mea}(\lambda)$ is calculated, the corrected shift in wavelength should be at a point where the correlation is maximum. Fig. 33 shows the correlation as a function of $\Delta\lambda$ from $\Delta\lambda = -5$ nm to $\Delta\lambda = 5$ nm. From this figure, the highest correlation is at $\Delta\lambda = 0$ which indicates that there is no shift in the monochromator calibration.

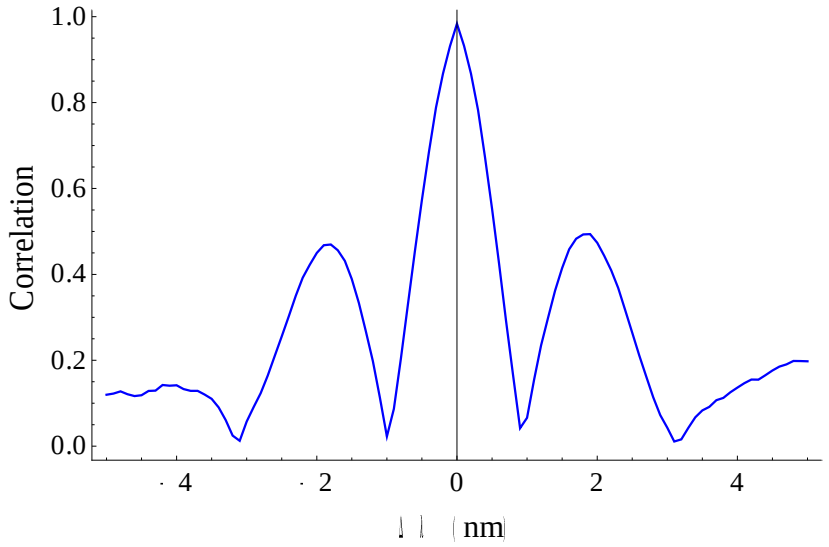

Figure 33 Correlation of $\boldsymbol{a_s\, S_{cal}(\lambda)}$ and $\boldsymbol{S_{mea}(\lambda)}$ as a function of wavelength shift $\boldsymbol{\Delta\lambda}$

4.5 Concentration Calculation Using Measured Reference $\boldsymbol{S_{mea}(\lambda)}$

The concentration for 2.6 ppm NO_2 gas can be extracted by fitting the measured optical density to the measured reference $S_{mea}(\lambda)$ and a 2nd order polynomial $P(\lambda) = \sum_{r=0}^{2} a_r\,(i - i_c)^{\,r}$

$$OD(i) = Ln\left[\frac{I_{2.6}(i)}{I_o(i)}\right] \cong a_s S_{mea}(i) + \sum_{r=0}^{2} a_r\,(i - i_c)^{\,r} \qquad (83).$$

According to section 2.6.7, X matrix is

$$\boldsymbol{X} = \begin{bmatrix} 1 & (-1500)^1 & (-1500)^2 & S_{mea}(0) \\ 1 & (1-1500)^1 & (1-1500)^2 & S_{mea}(1) \\ . & . & . & . \\ . & . & . & . \\ 1 & (2999-1500)^1 & (2999-1500)^2 & S_{mea}(2999) \end{bmatrix} \qquad (84),$$

The optical density vector $\overrightarrow{OD} \equiv \begin{bmatrix} OD(0) \\ OD(1) \\ . \\ . \\ OD(2999) \end{bmatrix}$, the parameter vector $\vec{a} \equiv \begin{bmatrix} a_o \\ a_1 \\ a_2 \\ a_s \end{bmatrix}$.

The fitting parameters can be calculated by

$$\vec{a} = [\boldsymbol{X}^T \boldsymbol{X}]^{-1} \boldsymbol{X}^T \overrightarrow{OD} \quad (85),$$

and their uncertainties are calculated by $\Delta a_j = \sqrt{\Theta_{jj}}$ with Θ_{jj} is calculated from Eq.54.

Fig. 34 shows the background spectrum $I_o(\lambda)$ and the signal spectrum of 2.6 ppm NO_2 $I_{2.6}(\lambda)$. The fitting parameters from this calculation are listed in Table 6 and the fitting results are shown in Fig. 35. Fig. 36 shows component of the 2th order of polynomial function.

Table 6 The fitting parameters calculated using the reference $\mathbf{S_{cal}}(\boldsymbol{\lambda})$ for the 2.6 NO_2 gas sample.

Scaling factor	Value	Uncertainty
a_s	0.01	0.002
a_0	-0.03	0.0001
a_1	1.8×10^{-6}	6.1×10^{-8}
a_2	6.2×10^{-10}	3.2×10^{-11}

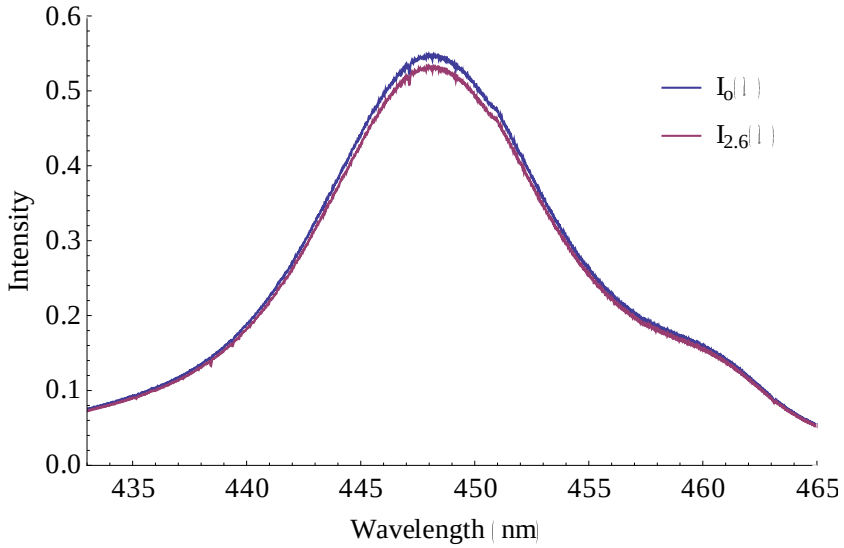

Figure 34 The background spectrum $\boldsymbol{I_o(\lambda)}$ (blue line) measured by admitting a pure N_2 gas into the gas cell and the signal spectrum $\boldsymbol{I_{2.6}(\lambda)}$ (red line) is measured by admitting a 2.6 ppm NO_2 gas into the cell.

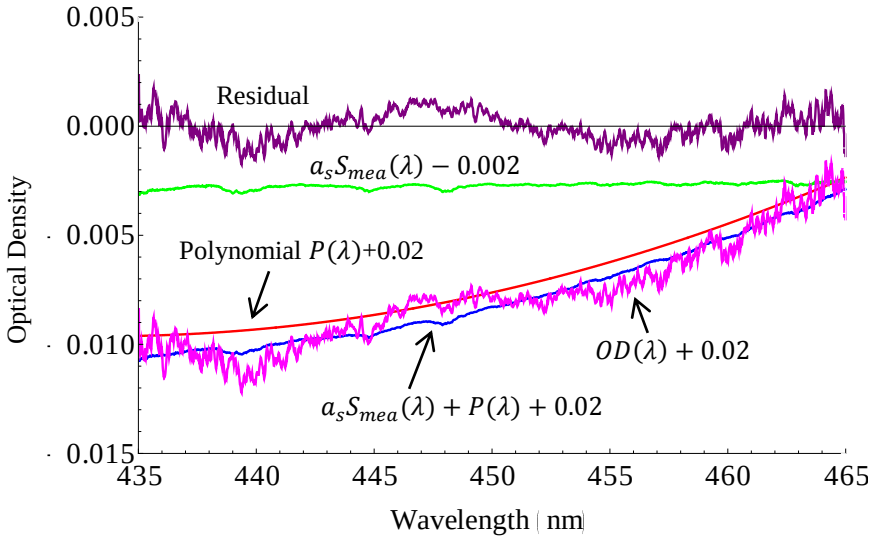

Figure 35 The measured optical density $\boldsymbol{OD(\lambda)}$, the scaled calculated reference $\boldsymbol{a_s S_{mea}}$, the polynomial function $\boldsymbol{P(\lambda) = a_0 + a_1\lambda + a_2\lambda^2}$, and the residual. For clarity purpose, three functions, $\boldsymbol{OD(\lambda)}$, $\boldsymbol{P(\lambda)}$ and $\boldsymbol{P(\lambda) + a_s S_{mea}(\lambda)}$, are shifted by 0.02 and the function $\boldsymbol{a_s S_{mea}(\lambda)}$ is shifted by -0.002.

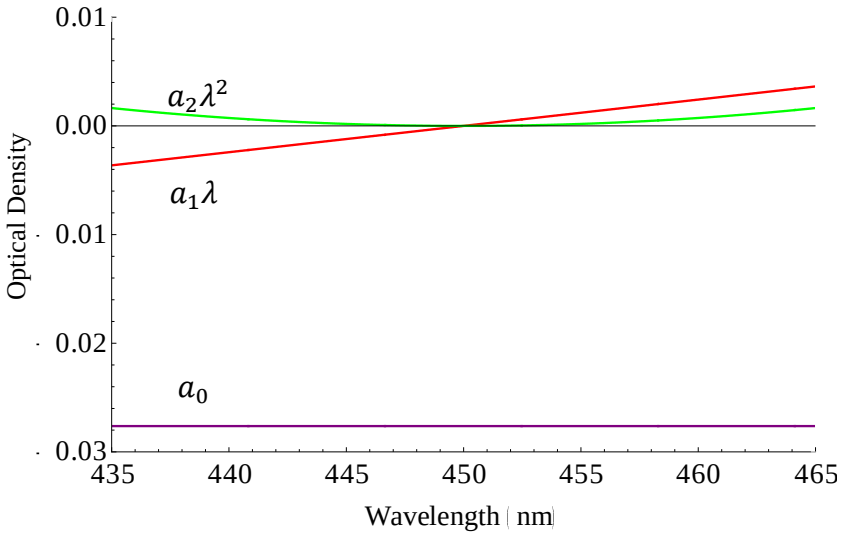

Figure 36 The components of the fitting polynomial function which is used for eliminating broad band profile in measured optical density.

The concentration of NO_2 gas at room temperature $T = 293\ K$ and room pressure $P = 1.1\ kPa$ can be calculated via Eq. 57:

$$c_{NO_2} = a_s \times \frac{7.9\ \alpha}{L} \times \frac{kT}{P} \times 10^6 \quad (86),$$

where the number 7.9 is scaling factor of $S_{mea}(\lambda)$ calculated in sec. 4.4.3.

$$c_{NO_2} = 0.01 \times \frac{7.9 \times 10^{16}}{15.5} \times \frac{1}{2.475 \times 10^{19}} \times 10^6 \quad (87),$$

$$c_{NO_2} = 2.4 \text{ ppm} \quad (88).$$

and the uncertainty of concentration can be calculated via Eq. 58:

$$\Delta c_{NO_2} = \Delta a_s \times \frac{7.9 \times \alpha}{L} \times \frac{kT}{P} \times 10^6 \quad (89),$$

$$\Delta c_{NO_2} = 0.003 \times \frac{7.9 \times 10^{16}}{15.5} \times \frac{1}{2.475 \times 10^{19}} \times 10^6 \quad (90),$$

$$\Delta c_{NO_2} = 0.5 \text{ ppm} \quad (91).$$

Thus the measured concentration is within 8 % of the quoted value, 2.6 ppm, by the gas cylinder supplier. Here we assume the length, the temperature and the pressure is known to a much better accuracy than 8%.

To examine the precision of DOAS method, ten concentration measurements of the 2.6 ppm NO_2 gas are performed under the same condition. The average value of concentration from these measurements is 2.6 ± 0.3 ppm with a confidence level of 95%, see Appendix C. The ten gas concentration measurements and their uncertainties are shown in Fig. 37 and listed in Table. 7.

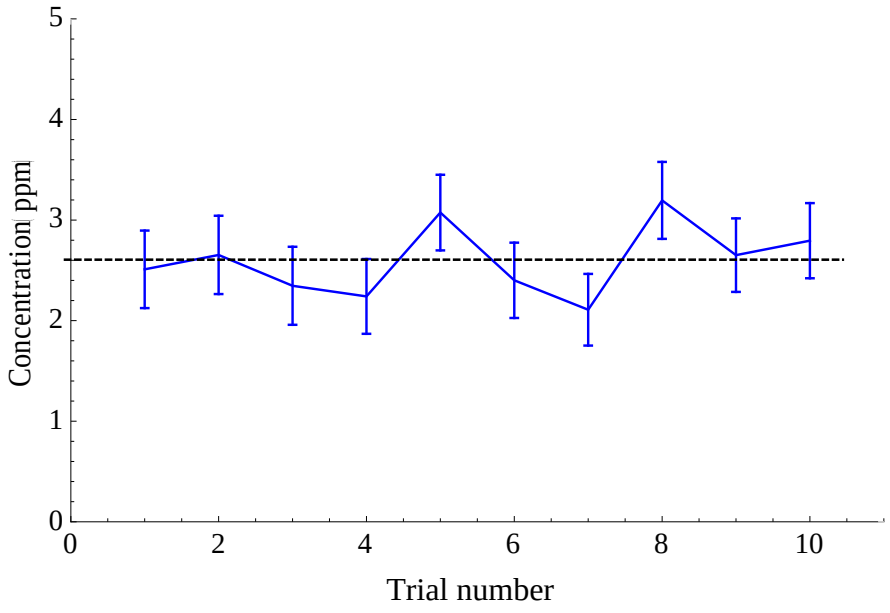

Figure 37 Gas concentration from different 10 measurements. The dashed line is quoted concentration (2.6 ppm) be the gas supplier.

Table 7 Concentration and its uncertainty for the 2.6 ppm NO_2 gas.

Trial number	Concentration (ppm)	Uncertainty (ppm)
1	2.6	0.4
2	2.7	0.4
3	2.4	0.4
4	2.3	0.4
5	3.1	0.4
6	2.4	0.4
7	2.1	0.4
8	3.2	0.4
9	2.7	0.4
10	2.8	0.4

4.6 Detection Limit

Detection limit can be estimated using equation [24]:

$$OD_{lim} \cong \delta_{DOAS} \times \frac{6}{\sqrt{n-1}} \quad (92),$$

where OD_{lim} is the smallest optical density that can be detected, δ_{DOAS} is the noise level of DOAS experimental setup and n is number of data points being used in the data analysis. δ_{DOAS} can be estimated from the standard deviation of the optical density $OD_o(\lambda) = Ln\left[\frac{I_o^1(\lambda)}{I_o^2(\lambda)}\right]$ calculated from two different background spectra $I_o^1(\lambda)\ and\ I_o^2(\lambda)$. Fig. 38 shows an example of such optical density. The standard deviation is calculated to be $\delta_{DOAS} = 3 \times 10^{-3}$.

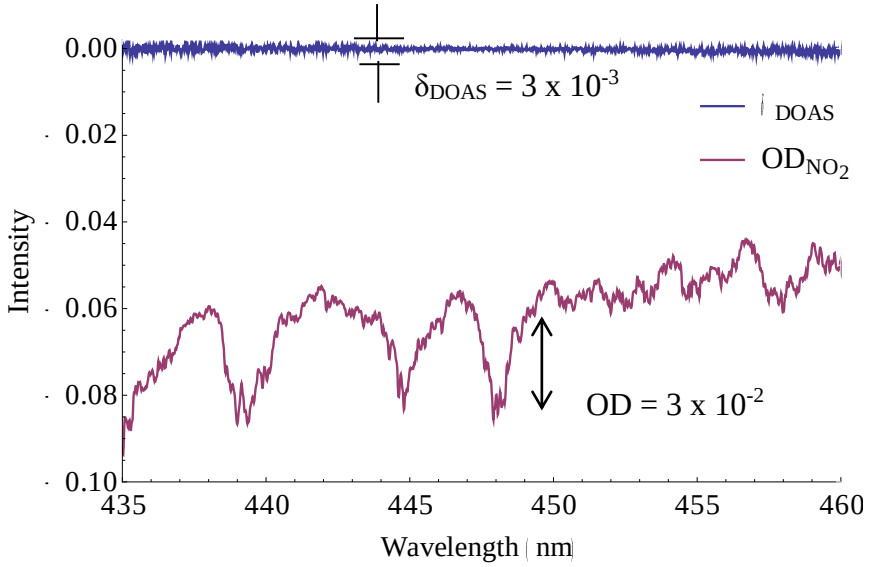

Figure 38 Noise level $\boldsymbol{\delta_{DOAS}}$ of DOAS experimental setup and NO_2 structure reference from 206 ppm.

In our analysis 2571 data points are used in the range of 435 – 465 nm. From these value then the smallest optical density that can be detected by our DOAS experimental setup is

$$OD_{lim} \cong 3 \times 10^{-3} \frac{6}{\sqrt{2571 - 1}} \cong 3.5 \times 10^{-4} \quad (93).$$

The optical density from a NO_2 gas with a concentration of 206 ppm is 0.03 (see Fig. 38).

So the smallest concentration that can be detected by our setup is

$$c_{lim} \cong \frac{3.5 \times 10^{-4}}{3 \times 10^{-2}} \times 206\, ppm \quad (94),$$

$$c_{lim} \cong 1.2\, ppm \quad (95).$$

CHAPTER 5

CONCLUSION AND RECOMMENDATIONS

5.1 Conclusion

In this thesis, we have employed DOAS method to determine very low NO_2 gas concentration. Our setup consists of a commercial white LED was used as the light source, a 15-cm gas cell, a high resolution monochromator, Horriba SPEX500M, coupled to a 3000-pixel CCD line camera, Thorlab LC1-USB CCD. A Labview program is developed to control and collect data and a Mathematica program is written to analyze the data.

Two NO_2 gas concentrations, 206 ppm and 2.6 ppm, are used to check the performance of our setup. Our measurements agree very well with the quoted concentration by the gas cylinders supplier. The deviation of our measurement for the case of the 206 ppm is less than 0.4 % while the deviation for the case of the 2.6 ppm is less than 8%. The detection limit is estimated to be ~1.2 ppm.

5.2 Future Work

Interesting results are obtained from this thesis and the following are some suggestions for further investigation:

1. Replace the gas cell in our DOAS setup with a long open-air path. With the detection limit we achieve for our setup which has a path length of 15.5 cm, a gas path of 300 m instead, for example, gives a detection limit of 0.6 ppb

which is much smaller than the 50 ppb recommended long-term exposure limit to NO_2 gas.

2. Investigate DOAS experimental setups using low resolution spectrometers which are cheaper and have more compact sizes.
3. Use blue LEDs with much higher intensities to improve statistics and reduce measurement time.

Appendix A.

Linearized Optical Density

Two approximation are used to derive Eq. 43

$$Ln[x] \approx x + 1 \quad \text{for } 1 - \epsilon < x < 1 + \epsilon \tag{A.1}$$

$$Exp[x] \approx 1 + x \ \text{ for } -\epsilon < x < \epsilon \tag{A.2}$$

In small concentration, the quantity $\sigma(\lambda).c.L \sim 0$, using this consideration, Eq. 42 can be written as

$$OD(\lambda) = Ln\left[\frac{1}{n''}\int_{\lambda''_{js}}^{\lambda''_{je}}\left\{\int_{-\Delta\lambda'}^{\Delta\lambda'} e^{-\sigma(\lambda''_i-\lambda')\,c.L}H(\lambda')\,d\lambda'\right\}d\lambda''\right] \tag{A.3}$$

$$OD(\lambda) \approx \frac{1}{n''}\int_{\lambda''_{js}}^{\lambda''_{je}}\left\{\int_{-\Delta\lambda'}^{\Delta\lambda'} e^{-\sigma(\lambda''_i-\lambda')\,c.L}H(\lambda')\,d\lambda'\right\}d\lambda'' - 1 \tag{A.4}$$

Convolution process is defined as

$$1 \cong \int_{-\Delta\lambda'}^{\Delta\lambda'} H(\lambda')\,d\lambda' \tag{A.5}$$

So Eq. A.4 can be written as

$$\begin{aligned} OD(\lambda) \approx \frac{1}{n''}\int_{\lambda''_{js}}^{\lambda''_{je}}\left\{\int_{-\Delta\lambda'}^{\Delta\lambda'} e^{-\sigma(\lambda''_i-\lambda')\,c.L}H(\lambda')\,d\lambda'\right\}d\lambda'' \\ -\frac{1}{n''}\int_{\lambda''_{js}}^{\lambda''_{je}}\left\{\int_{-\Delta\lambda'}^{\Delta\lambda'} H(\lambda')\,d\lambda'\right\}d\lambda'' \end{aligned} \tag{A.6}$$

$$OD(\lambda) \approx \frac{1}{n''}\int_{\lambda''_{js}}^{\lambda''_{je}}\left\{\int_{-\Delta\lambda'}^{\Delta\lambda'}\left\{e^{-\sigma(\lambda''_i-\lambda')\,c.L} - 1\right\}H(\lambda')\,d\lambda'\right\}d\lambda'' \tag{A.7}$$

Applying Eq. A.2 , then we have a linear expression

$$OD(\lambda) \approx \frac{1}{n''}\int_{\lambda''_{js}}^{\lambda''_{je}}\left\{\int_{-\Delta\lambda'}^{\Delta\lambda'}\{-\sigma(\lambda''_i-\lambda')\,c.L\}H(\lambda')\,d\lambda'\right\}d\lambda'' \quad \text{A.8}$$

$$OD(\lambda) \approx \frac{c.L}{\alpha}\frac{1}{n''}\int_{\lambda''_{js}}^{\lambda''_{je}}\left\{\int_{-\Delta\lambda'}^{\Delta\lambda'}\{-\sigma(\lambda''_i-\lambda')\,\alpha\}H(\lambda')\,d\lambda'\right\}d\lambda'' \quad \text{A.9}$$

Eq. A.6 is a linear expression of NO_2 optical density which states that optical density of particular concentration c can be approached as linear function of reference with column density α by scaling factor $\frac{c.\ L}{\alpha}$.

Next step of derivation, approximation of exponential function (Eq, A.1, Eq. A.2) is applied again but now with reverse direction.

$$OD(\lambda) \approx \frac{c.L}{\alpha}\frac{1}{n''}\int_{\lambda''_{js}}^{\lambda''_{je}}\left\{\int_{-\Delta\lambda'}^{\Delta\lambda'}\left\{e^{-\sigma(\lambda''_i-\lambda')\,\alpha}-1\right\}H(\lambda')\,d\lambda'\right\}d\lambda'' \quad \text{A.10}$$

$$OD(\lambda) \approx \frac{c.L}{\alpha}\frac{1}{n''}\int_{\lambda''_{js}}^{\lambda''_{je}}\left\{\int_{-\Delta\lambda'}^{\Delta\lambda'}e^{-\sigma(\lambda''_i-\lambda')\,\alpha}H(\lambda')\,d\lambda'\right\}d\lambda'' - \frac{c.L}{\alpha}\frac{1}{n''}\int_{\lambda''_{js}}^{\lambda''_{je}}\left\{\int_{-\Delta\lambda'}^{\Delta\lambda'}H(\lambda')\,d\lambda'\right\}d\lambda'' \quad \text{A.11}$$

$$OD(\lambda) = \frac{c.L}{\alpha}Ln\left[\frac{1}{n''}\int_{\lambda''_{js}}^{\lambda''_{je}}\left\{\int_{-\Delta\lambda'}^{\Delta\lambda'}e^{-\sigma(\lambda''_i-\lambda')\,\alpha}H(\lambda')\,d\lambda'\right\}d\lambda''\right] \quad \text{A.12}$$

Appendix B

Mathematica Codes

Data analysis in this work was done by writing a code in Mathematica software [30]. Some functions were built and listed as follows

1) $addSpectra\ [I_1(\lambda), I_2(\lambda), a]$

This function calculates an addition of two spectrum with a scale *a*.

$addSpectra[I_1(\lambda), I_2(\lambda), a] \rightarrow I_1(\lambda) + a.I_2(\lambda)$

```
addSpectra[list1_, list2_, multiply_] := Module[{sum},
  sum = Table[{list1[[i, 1]], list1[[i, 2]] + multiply*list2[[i, 2]]}, {i, 1, Length[list1]}];
  Return[sum];
  ]
```

2) $buildX[polinomial\ order, \{S_i(i), \dots\}]$

This function builds an X matrix according to Eq. 45

$$buildX[2, \{S_1(i), S_2(i)\}] \rightarrow \begin{bmatrix} 1 & (-i_c)^1 & (-i_c)^2 & S_1(0) & S_2(0) \\ 1 & (1-i_c)^1 & (1-i_c)^2 & S_1(1) & S_2(1) \\ . & . & . & . & \\ . & . & . & . & \\ 1 & (n-i_c)^1 & (n-i_c)^2 & S_1(n) & S_2(\mathrm{n}) \end{bmatrix}$$

$with\ i_c = n/2$

```
buildX[order_, list_] := Module[{var, numVar, length, ic, XT, X, j, l},
(*number of reference included in X matrix *)
  numVar = Length[list];
(*Length of list*)
  length = Length[list[[1]]];
(*center of pixel is defined as half of list length *)
  ic = Round[length/2];
(*Initiate a blank XT matrix*)
  XT = {};
(*building polinomial*)
  For[j = 0, j <= order, j++,
   If[j == 0, var = Table[1, {i, 1, length}],
    var = Table[(i - ic)^j, {i, 1, length}]];
   XT = Append[XT, var];
   ];
(*inserting references*)
  For[l = 1, l <= numVar, l++,
   var = Table[list[[l]][[i, 2]], {i, 1, length}];
   XT = Append[XT, var];
   ];
(*X matrix is tranpose of XT*)
  X = Transpose[XT];
    Return[X]
  ]
```

3) $correlation[f_1(\lambda), f_2(\lambda)]$

This function calculates correlation between two functions.

$$correlation[f_1(\lambda), f_2(\lambda)] \rightarrow \frac{covariance[f_1(\lambda), f_2(\lambda)]}{\delta_1 \delta_2}$$

$$with\ \delta_1 and\ \delta_2\ are\ standard\ deviation\ of\ f_1(\lambda) and\ f_2(\lambda)$$

```
correlation[list1_, list2_] :=
 Module[{x, y, cova, stdX, stdY, correlated},
  x = Table[list1[[i, 2]], {i, 1, Length[list1]}];
  y = Table[list2[[i, 2]], {i, 1, Length[list2]}];
  cova = Covariance[x, y];
  stdX = StandardDeviation[x];
  stdY = StandardDeviation[y];
  correlated = (1.0*cova)/(stdX*stdY);
  Return[correlated];
  ]
```

4) $calLog[f_1(\lambda)]$

This function calculates natural logarithm of a function.
$calLog[f_1(\lambda)] \rightarrow Ln[f_1(\lambda)]$

```
calLog[list_] := Module[{lst},
  lst = Table[{list[[i, 1]], Log[list[[i, 2]]]}, {i, 1, Length[list]}];
  Return[lst];
  ]
```

5) $lSQ[X, f(\lambda)]$

This function calculates scaling factors by least square fitting according to Eq. 44.

$$lSQ[X, f(\lambda)] \rightarrow \left[\boldsymbol{X}^T\boldsymbol{X}\right]^{-1}\boldsymbol{X}^T\vec{f}(\lambda)$$

```
lSQ[X_, listY_] :=
 Module[{XT, a, n, m, σ2, Θ, Δa},
  XT = Transpose[X];
  Off[Inverse::luc];
  a = Inverse[XT.X].XT.listY[[All, 2]]; (* calculate scaling factors Eq. 44*)
  m = Dimensions[X][[2]];                (* number of column in X matrix*)
  n = Dimensions[X][[1]];                (* number of row in X matrix*)
  σ2 = (1/(n - m))*((listY[[All, 2]] - X.a).(listY[[All, 2]] -X.a)); (* calculate error Eq. 46*)
  Θ = σ2*Inverse[XT.X];                  (* calculate covariance matrix Eq. 47*)
  Δa  = Table[Sqrt[Θ [[i, i]]], {i, 1, m}];   (* calculate error of scaling factor Eq. 48*)
  Return[{a, Δa }];
  ]
```

6) $multiply[f_1(\lambda), number, power]$

This function calculate multiplication of a function with some function.

$$multiplySP[f_1(\lambda), a, b] \rightarrow f_1(\lambda) * a^b$$

```
multiply[list_, number_, pow_] := Module[{multiList},
  multiList =
   Table[{list[[i, 1]], number^pow*list[[i, 2]]}, {i, 1,
     Length[list]}];
  Return[multiList]
  ]
```

7) $multiplySP[f_1(\lambda), f_2(\lambda), power]$

This function calculate multiplication of two function.

$$multiplySP[f_1(\lambda), f_2(\lambda), a] \rightarrow f_1(\lambda) * f_2(\lambda)^a$$

```
multiplySp[list1_, list2_, num_] := Module[{multiList},
  multiList =
   Table[{list1[[i, 1]], list1[[i, 2]]*list2[[i, 2]]^num}, {i, 1, Length[list1]}];
  Return[multiList]
  ]
```

8) $pTo\lambda[f(i)]$

This function convert pixel into wavelength according Eq. 62.

$pTo\lambda[f(i)] \rightarrow f(432.477 + 0.0117 * i)$

```
pTo\u03bb [list_] := Module[{lst, p, pixel},
  (*p[pixel_]:=Module[{},432.477+0.0117*pixel]; *)
    lst = ToExpression[Table[{p[list[[i, 1]]], list[[i, 2]]}, {i, 1, Length[list]}]];
  Return[lst];
  ]
```

9) $readTheses[number]$

This function reads data file theses_number.lvm

$readTheses[100] \rightarrow read\ data\ from\ theses\_100.lvm$

```
readTheses[num_] := Module[{sNum, stream, lst0, lst},
  SetDirectory[NotebookDirectory[]];
  sNum = ToString[num];
  stream = OpenRead["Theses_" <> sNum <> ".lvm"];
  lst0 = ReadList[stream, Record];
  Close[stream];
  lst = ToExpression[
    Table[{StringSplit[lst0[[i]], ","][[1]],StringSplit[lst0[[i]], ","][[2]]}, {i, 1, Length[lst0]}]];
  lst = pTo\u03bb[lst];
  Return[lst];
  ]
```

10) $selectSpectra[f(\lambda), \lambda_1, \lambda_2]$

This function will select a function $f(\lambda)$ from $\lambda_1\ to\ \lambda_2$

$selectSpectra[f(\lambda), 435\ ,465\ ] \rightarrow f(\lambda)|\lambda_0 = 435\ nm\ and\ \lambda_n = 465\ nm$

```
selectSpectra[list_, min_, max_] := Module[{lst},
  lst = Select[list, First[#] >= min && First[#] <= max &];
  Return[lst];
  ]
```

11) $smooth[f(\lambda)]$

This function smooth a function by averaging 8 consecutives point.

```
smooth[list_] := Module[{dummy, smoothed, pre, post, comb},
  dummy = list[[All, 2]];
  pre = Table[dummy[[i]], {i, 1, 3}];
  post = Table[dummy[[i]], {i, Length[list] - 3, Length[list]}];
  dummy = MovingAverage[dummy, 8];
  comb = Join[pre, dummy, post];
  smoothed = Table[{list[[i, 1]], comb[[i]]}, {i, 1, Length[list]}];
  Return[smoothed];
  ]
```

12) $\delta\lambda[f(\lambda), \lambda_i, direction]$

This function calculate difference of two wavelength point:

$\delta\lambda[f(\lambda), 450, a] \rightarrow f(450 + a) - f(450)$

```
δλ[list_, i_, mult_] := Module[{δ},
  δ = list[[i + mult*1, 1]] - list[[i, 1]];
  Return[δ]
  ]
```

13) $H[f(\lambda), \lambda_i, \lambda_j, resolution]$

This function calculate Gaussian function for particular points and resolution:

$$H[f(\lambda), \lambda_1, \lambda_2, res] \rightarrow Exp\left[-\frac{(\lambda_1 - \lambda_2)^2}{2\,res^2}\right]$$

```
H[list_, i_, j_, res_] :=
  Module[{h, δλ, value},
   h = Exp[-((list[[i, 1]] - list[[j, 1]])^2/(2 res^2))];
   Return[h]
];
```

14) $expo[f(\lambda), \lambda_j]$

This function calculate exponential of a function:

$expo[f(\lambda), \lambda_1] \rightarrow Exp[f(\lambda_1)]$

```
expo[list_, i_] := Module[{absorbed},
   absorbed = Exp[-list[[i, 2]]];
   Return[absorbed];
   ];
```

15) $makeS[\sigma(\lambda), \lambda_s, \lambda_e, \Delta\lambda, \alpha, resolution]$

This function calculate absorption reference using high-resolution cross-section database Eq. 52:

$$makeS[\sigma(\lambda), \lambda_s, \lambda_e, \Delta\lambda, \alpha, res] \rightarrow S(\lambda|\lambda_s \rightarrow \lambda_e): Ln\left[\frac{1}{n''}\sum_{j=js}^{je}\int_{-\Delta\lambda'}^{\Delta\lambda'} e^{-\sigma\left(\lambda_j^{ref}-\lambda'\right)\alpha} H\left(\lambda', res\right)\, d\lambda'\right]$$

```
makeS[crosList_, begin_, end_, width_, α_, res_] :=
  Module[{σ, list, min, max, maxNum, minNum, pos, i, num,
    denum, convDum, num1, num2, denum1, denum2, cros, Δλ, convolution},
cros = crosList;
cros = selectSpectra[cros, begin - width/2., end + width/2.];
cros = multiply[cros, α, 1];
list = selectSpectra[cros, begin, end];
maxNum = Length[list]; convDum = {};

For[minNum = 1, minNum <= maxNum, minNum++,
σ = selectSpectra[cros, list[[minNum, 1]] - 1.5*width, list[[minNum, 1]] + 1.5*width];
pos = Position[σ [[All, 1]], Select[σ, First[#] >= list[[minNum, 1]] &, 1][[1]][[
1]]][[1]][[1]];
Δλ = 0; i = 0; num = 0; denum = 0;
While[Δλ <= (width/3.),
num1 = expo[σ, pos - i] H[σ, pos - i, pos,res] Δλ [ σ, pos - i, -1];
     If[i <= 0, num2 = 0,
      num2 = expo[σ, pos + i] H[σ, pos + i, pos, res] Δλ [ σ, pos + i, -1];
      ];
     num = num1 + num2 + num;
     denum1 = H[σ, pos - i, pos, res] Δλ [ σ, pos - i, -1];
     If[i <= 0, denum2 = 0,  denum2 =  H[σ, pos + i, pos, res] Δλ [ σ, pos + i, -1];
      ];
     denum = denum1 + denum2 + denum;
     i = i + 1;
     Δλ = σ [[pos + i, 1]] - σ [[pos, 1]];
     ];
    convDum = Append[convDum, num/denum];
    ];
   convolution = Table[{list[[i, 1]], convDum[[i]]}, {i, 1, Length[list]}];
   Return[convolution]
   ];
```

16) $callDoas[I_o(\lambda), S(\lambda), I(\lambda), \lambda_s, \lambda_e, h, \Delta\lambda]$

This is a doas analysis function as explained in Fig. 12:

```
callDoas[listIo_, listS_, listI_, begin_, end_, h_, Δλ_] :=
  Module[{Io, Ii, Jo, Ji, S, result},
(* assign background spectra *)
Io = listIo;
(*shift background spectra*)
  Io[[All, 1]] = Io[[All, 1]] + Δλ;
(* select on particular wavelength range*)
  Io = selectSpectra[Io, begin, end];
(* assign transmitted spectra*)
  Ii = listI;
(*shift transmitted spectra*)
  Ii[[All, 1]] = Ii[[All, 1]] + Δλ;
(*select transmitted spectra on particular wavelength range*)
  Ii = selectSpectra[Ii, begin, end];
(*assign reference spectra*)
  S = listS;
(*select particular wavelength range*)
  S = selectSpectra[S, begin, end];
(* calculate natural logarithm of spectra*)
  Jo = calLog[Io];
  Ji = calLog[Ii];

(* calculate optical density*)
oD=addSpectra[J,Jo,-1];
(*smoothing optical density*)
oD=smooth[oD];
(*Build X matrix*)
X=buildX[h,{S}];

(*least square fitting*)
{a,Δa}=lSQ[X,oD];

  Return[{a,Δa}];
  ]
```

Appendix C

Error Propagation

The uncertainty of several measurement could be calculated by

$$\sigma_x^2 \cong \sigma_u^2 \left[\frac{\partial x}{\partial u}\right]^2 + \sigma_v^2 \left[\frac{\partial x}{\partial v}\right]^2 + \cdots \quad \text{(D.1)}$$

With σ_u, σ_v, ... are individual uncertainties from individual measurements u, v, ...

For example, we want to calculate the uncertainty of average value from n number of measurements I_i:

$$\bar{I} = \frac{1}{n}\sum_{i=1}^{n} I_i \quad \text{(D.2)}$$

Then the uncertainty is given by

$$\sigma_F^2 = \sum_{i=1}^{n} \sigma_i^2 \left[\frac{\partial \bar{I}}{\partial I_i}\right]^2 \quad \text{(D.3)}$$

$$\sigma_F^2 = \frac{1}{n^2}\sum_{i=1}^{n} \sigma_i^2$$

If σ_i^2 is almost the same for all measurement, then we have

$$\sigma_F = \frac{\sigma_i}{\sqrt{n}} \quad \text{(D.2)}$$

Then true value lies within the range

$$I = \bar{I} \pm 1.96\, \sigma_F \quad \text{(D.2)}$$

With 95% confidence level.

Appendix D

LC1-USB CCD Camera

A Charge coupled device or CCD camera is a device that record photon which falls in its pixel [32]. Pixel is a photon sensitive element which is made of integrated circuit on the silicon surface. Incident photon would generate charge, which is called photoelectric effect, and then read as digital number. CCD camera working principle can be simplified by seeing as an array of bucket (pixel) and incoming photon as rainwater. Each bucket exposed to rain for the same amount of time (integration time). Then the amount of water in each bucket was stored as spectral data.

Figure E.1 LC1-USB CCD Camera [31]

In this theses, we used LC1-USB CCD Camera produced by THORLAB.inc. The specification of this CCD camera is shown in Table below.

Detector Range (CCD)	350 – 1000 nm
CCD Pixel Size	7 µm x 200 µm
CCD Sensitivity	300 V/ lx.s
CCD Pixel Number	3000
Integration Time	1 µs – 200 ms

Electronic Offset Correction

Electronic offset is a signal produced by CCD camera to avoid a negative signal at very low intensity. This phenomena can be corrected using spectrum from the lowest integration time with no light entering CCD camera

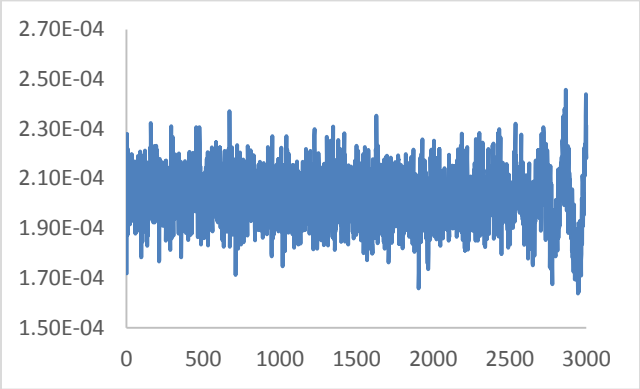

Figure E.2 Electronic offset correction for LC1- CCD Camera

Dark Current

Dark current is produced by thermally excited electron in CCD camera electronic system. Dark current can easily be corrected by recording spectra in dark condition with time integration is the same as in the experiment.

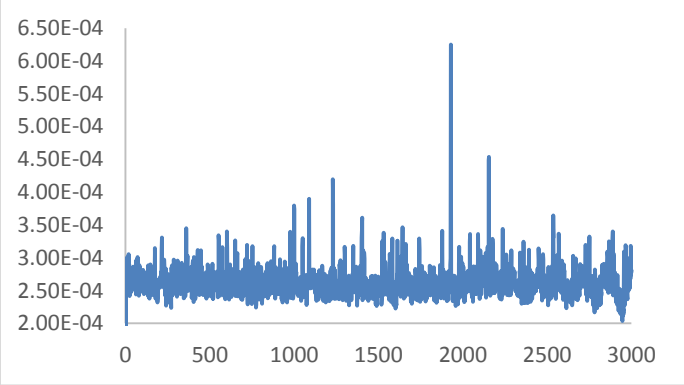

Figure E.3 Dark Current correction for LC1-USB CCD camera

References

[1] United States Environmental Protection Agency, "Latest Findings on National Air Quality," *U.S. EPA Report EPA-454/R-07-007,* pp. 5, Jan, 2008.

[2] D.S Lee, I. Kohler, E. Grobler, et.al,"Estimations of Global NO_x Emission and Their Uncertainties" Atmospheric Environment Vol.31. No. 12, pp 1735-1749, 1997.

[3] Elke Stehfest, Lex Bouwman, "N_2O and NO emission from agricultural fields and soil".Nutrient cycling in Agroecosystem 74, pp. 207-228, 2006

[4] United States Environmental Protection Agency, "Our Nation's Air-Status and Trends through 2008," *U.S. EPA Report EP-D-05-004,* pp. 31, Feb, 2010.

[5] W. James Gauderman, Edward Avol, Fred Lurmann,"Childhood Astma and Exposure to Traffic and Nitrogen Dioxide", Epidemiology No.16 pp.737-743,2005.

[6] Jennifer A. Logan, Michael J. Prather, Steven C. Wofsy et. all, "Tropospheric Chemistry: A Global Prespective",Journal of Geophysical Research, Vol.86 pp.7210-7254, 1981.

[7] Demerjian, K.,L.,"A review of national monitoring networks in North America". Atmos. Environ., 34 1861-1884. 2000.

[8] Atkinson, R., "Atmospheric chemistry of VOCs and NO_x". Atmos.Environ. 34 2063-2101. 2000.

[9] Weissbluth Mitchel," Atoms and Molecules",Academic Press,Inc.1978.

[10] Wilkinson,I., Whitaker, B.,J.,"Some remarks on the photodynamics of NO_2", Annu. Rep. Prog. Chem., Sect. C, 106 274-304. 2010.

[11] S.Voight, J. Orphal, J.P. Burrows." The temperature and pressure dependence of the absorption cross-sections of NO_2 in the 250-800 nm region measured by Fourier-transform spectroscopy". Journal of Photochemistry and Photobiology A: Chemistry 149 (2002) 1-7

[12] K. Yoshino, J.R. Esmond, W.H. Parkinson,"High resolution absorption cross section measurement of NO_2 in the UV and visible region", Chemical Physics Vol.221 pp. 169-174. 1997.

[13] Wilkinson,I., et.all., "The photodissociation of NO_2 by visible and ultraviolet light", Phys. Chem. Chem. Phys. 12 15766-15779. 2010.

[14] Bohren,C.F., D.R.Huffman, "Absorption and scattering of light by small particles". John Wiley&Son, New York, 1983.

[15] U. Platt, J.Stutz."Differential Optical Absorption Spectroscopy". Springer. pp.95 2008.

[16] Lampel J., et.all.,"The impact of vibrational Raman scattering of air on DOAS measurements of atmospheric trace gases", Atmos. Meas. Tech. Discuss. 8 3423-3469. 2015

[17] Perner,D., Platt, U., J.S."Detection of nitrous acid in the atmosphere by differential optical absorption". Geophys. Res. Lett. Vol. 6, 917-920.1979

[18] Plat,U., Perner.,D."Direct measurement of Atmospheric CH_2O, HNO_2, O_3, NO_3 and SO_2 by differential optical absorption in the Near UV", J. Geophys. Res. 85, 7453-7458. 1979.

[19] Platt,U., D. Perner,"Detection of NO_3 in the polluted trophosphere by differential optical absorption", Geophys. Res. Lett. 7, 89-92. 1980.

[20] Sander,R.W.Solomon.S.,,"Ground based measurement of O_3, NO_2, OClO and BrO during the antartic ozone depletion event.". Quadrennial ozone symposium 1988. Pp. 65-70. 1988.

[21] Alicke, B., K. Heberstreit, J. Stutz and Platt U., " Iodine oxide in the marine boundary layer"., Nature 397, 572-573 . 1999.

[22] Chan Ka-Lok, Ling Liy-Yi, Andreas Harti, et all.," Comparing different light-emitting diodes as light sources for long path differential optical absorption spectroscopy NO_2 and SO_2 measurements" Chin. Phys. B Vol.21 No.11 2012. pp.119301

[23] Volkamer, T., P. Spietz, Burrows, J.P. " DOAS measurement of glyoxal as an indicator for fast VOC chemistry in urban air." Geophys. Res. Lett. 32. 2005.

[24] Burrows J.P., Platt U., "The Remote Sensing of Tropospheric Composition from Space", Springer – Verlag Berlin Heidelberg. 2011.

[25] Stutz J., Platt U.,"Numerical analysis and estimation of the statistical error of differential optical absorption spectroscopy measurements with least-squares methods". Applied Optics. Vol.35 No.30 pp. 6041-6053. 1996.

[26] Bevinton,P.R.,Robinson,D.K.,"Data Reduction and Error Analysis 3rd edition", McGraw-Hill.New York.2003.

[27] Heij,C., Boer de P., Franses H.P., " Econometric Methods with Application in Business and Economics", Oxford University Press.2004.

[28] Reader, J., Corliss, C.H." Wavelengths and Transition Probabilities for Atoms and Atomic Ions". National Standard Reference Data System, National Bureau of Standards.1980.

[29] http://www.ni.com/labview/, accessed at April,21 2015.

[30] Wolfram Research, Wolfram Mathematica® 9. 2012.

[31] Thorlab Instrumentation,"LC1-USB Line Camer: Operation Manual",www.thorlab.de. 2010.

[32] http://www.specinst.com/What_Is_A_CCD.html, accessed at April,21 2015.

Vitae

Name	:Moch Syarif Romadhon
Nationality	:Indonesia
Date of Birth	:7/3/1983
Email	:syarif.romadhon@yahoo.com
Address	:Poncowolo Timur I/412 Semarang 50131 Indonesia
Academic Background	:B.Sc. in Physics at Institut Teknologi Bandung, Indonesia